Enhanced Adsorption of Methylene Blue Using Modified Coal Gasification Coarse Slag

Shuai Li

Student ID: 20319566

Department of Chemical and Environmental Engineering

University of Nottingham Ningbo China

Submitted May 2022, in partial fulfillment of

the conditions of the award of the degree MRes. in

Environmental Science and Engineering

I hereby declare that this dissertation is all my own work, except as

indicated in the text:

Signature: _____

Date: _____/_____/____

ABSTRACT

Huge amount of coal gasification coarse slag (CGCS) is produced every year as a by-product of the coal gasification process. Currently, most of the CGCS in China is disposed of in landfills, which not only occupies vast areas of land but also poses potential environmental risks, e.g., leaching of heavy metals and other pollutants contained wherein. Therefore, alternative approaches to achieve safe disposal and even resource utilization of CGCS are in urgent need.

In this study, we developed an experimental protocol to convert CGCS into mesoporous carbon–silicon composite (CGCS–CSC) from CGCS after ball mill (CGCS–BM) for the adsorbent of methylene blue (MB). The CGCS is firstly leached by an acid to remove the metal oxides and is then calcinated with an alkaline to activate the carbonaceous components and silica in the slag to form mesoporous carbon-silicon composite. The effects of various acids and calcination temperature on the pore structure were investigated. The structures, morphology, and properties of the as-prepared CGCS–CSC were characterized using various analytical methods, e.g., XRD, BET, SEM, TEM, FTIR, TGA, and XRF. Then, the MB adsorption performance of the CGCS–CSC for MB was evaluated experimentally and compared with those predicted by the response surface methodology (RSM). Moreover, the kinetics and thermodynamics of the adsorption process were systematically analyzed.

The BET results reveal that the as-prepared CGCS–CSC exhibits a much higher BET surface area than CGCS–BM, i.e., 438 m^2/g and 116 m^2/g, respectively. On the other hand, the SEM images indicate that after the treatments, the morphology of CGCS–BM

was converted from a large flaky shape to granules with well–developed pores. The comparisons between the experimental and simulation results demonstrate that the RSM can accurately predict the removal capacity of CGCS–CSC for MB. Guided by the RSM, the maximum adsorption amount of MB (i.e., 556 mg/g) could be achieved when 0.5 g/L CGCS–CSC is added to a 300 mg/L MB solution at pH = 7, room temperature for 3 hours.

The kinetics study indicates that the adsorption process of MB using CGCS–CSC fits very well with the Langmuir model and follows the first–order kinetics. This suggests that the adsorption process of MB by CGCS–CSC is a monomolecular layer of physical adsorption. This is mainly caused by electrostatic interaction, i.e., via surface-active group (e.g., silica hydroxyl group) and hydrogen bonding (3450 and 1010 cm^{-1}) that is evidenced by TGA and FTIR measurements, respectively. The TGA results indicate that amount of silica hydroxyl group on the as–prepared CGCS–CSC is between 24.0 and 26.5 $/nm^2$, much larger than those reported by other researchers.

Keywords: Coal Gasification Coarse Slag (CGCS), Carbon-silicon Composite (CSC), Response Surface Methodology (RSM), Methylene Blue (MB)

ACKNOWLEDGEMENTS

I would like to express my heartfelt gratitude to those who guide me through my MRes studies. They shared their experiences without reservation that cultivated my ability, increased my wisdom, and enabled me to successfully complete my research.

Firstly, I would like to express my sincere gratitude to my first supervisor, Dr. Mengxia Xu. Without his patient guidance, I would not be able to have successfully completed my MRes degree. I am also grateful to my second supervisor, Prof. Tao Wu, for guiding me during the regular group meetings. I want to thank my third supervisor, Dr. Xiang Luo as well for his assistance in the lab. Besides, I would like to thank my internal examiner Dr. Kow Kien Woh and external examiner Dr. Xinbao Li from Ningbo University for their constructive comments on my thesis.

TABLE OF CONTENT

LIST OF FIGURES

LIST OF TABLES

ACHIEVEMENTS

Journal Paper

Dawei Lan, Huiwen Zhu, Jianwen Zhang, **<u>Shuai Li</u>**, Quhan Chen, Chenxi Wang, Tao Wu, Mengxia Xu. Adsorptive removal of organic dyes via porous materials for wastewater treatment in recent decades: A review on species, mechanisms and perspectives. Chemosphere, 2022, 293: 133464.

Patent

Mengxia Xu, **<u>Shuai Li</u>**, Tao Wu, Peng Jiang, Xiang Luo. A method of preparing carbon–silicon composites using coal gasification coarse slag (filed, application number: 202210501032.4)

1. BACKGROUND

1.1. Coal Gasification Coarse Slag (CGCS)

Coal gasification coarse slag (CGCS) is the main solid waste produced by the reaction of coal with air, oxygen, and water vapor at a certain temperature and pressure [1]. Its main constituents are SiO_2, Al_2O_3, CaO, Fe_2O_3, and residual carbon. The compositional composition is determined by the process parameters of coal gasification and the feeding technology. As shown in Figure 1.1, the crude slag is collected in the lock hopper under high temperature and pressure after crushing and cooling operations, and then discharged through the slag discharge port, accounting for 75–80% of the total gasification slag by mass. The discharge process also requires dewatering by weight through a dredge for easy storage.
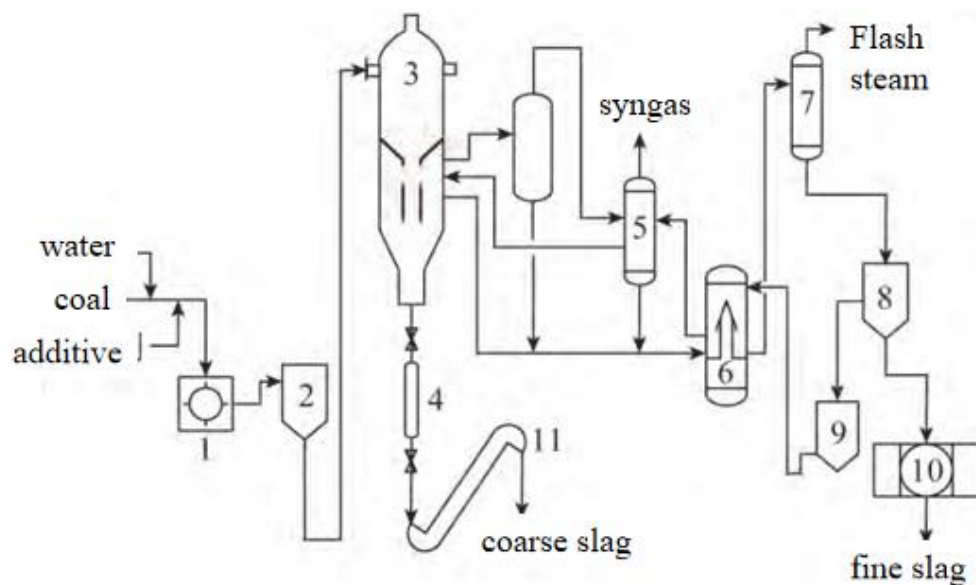
1–coal mill; 2–coal paddle groove; 3–multi–nozzle opposite type gasifier; 4–lock hopper; 5–water washing tower; 6–evaporative hot water tower; 7–vacuum flash evaporator; 8–clarifying tank; 9–gray water tank; 10–vacuum filter; 11–dregs machine

Figure 1.1 Multi–nozzle opposed coal–water slurry gasification proces [1].

The coal gasification process will produce fine slag in addition to coarse slag. The fine slag is cleaned, precipitated, and collected in gas form in the de–dusting unit of the syngas and dewatered by vacuum filtration. Therefore, there is a considerable difference between coarse and fine slag. First of all, the yield is the most obvious difference. According to the data [2], three–quarters of the gasification slag is CGCS, while the fine slag accounts for only a quarter, with a content ratio of about 3:1. Second, their surface structure is slightly different. The surface of coarse slag can be smooth and dense spherical particles, stacked lumps, irregular porous particles, etc., while fine slag is a combination of spherical particles, isolated giant spheres, and irregular porous particles. Third, the porosity of coarse slag is lower than that of fine slag, but the average porosity is high. Fourth, they differ in the amount of residual carbon they contain. The carbon content in the coarse slag is smaller than that in the fine slag, presumably because the residence time of the fine slag in the furnace is shorter than that of the coarse slag, part of the residual carbon particles and fine mineral particles are entrained by the syngas . The carbon content of the fine slag is higher because some of the residual carbon particles and fine mineral particles are discharged from the syngas outlet under the entrainment of syngas [3]. In the range of 105–280 μm, the carbon concentration is greater than 50%, while the opposite is true for fine slag. In addition, fine slag consists of stable carbon and is difficult to ignite [4]. These differences in properties can help in selecting samples and designing experiments.

Currently, the use of coal gasification ash and slag has become one of the main obstacles to the development of the coal chemical sector. A megaton coal indirect oil production facility may generate more than 600,000 tons of gasification ash per year [5]. To date, annual ash emissions from the Chinese coal chemical industry have been as high as 33

million tons [6]. If these wastes are dumped without proper treatment, they contain hazardous compounds that may create biological toxicity and environmental risks in the environment.

Different types of furnaces produce CGCS, which consists of two main types of structures: coal coke, a fusible inert material produced by a series of chemical reactions at high temperatures, and spongy, porous residual carbon structures. CGCS consists of small, dense, amorphous glass-phase particles and compact solids with macroscopic lamellar structures. CGCS has a wide size distribution, mostly between 1000 and 4000 μm, when it contains a high proportion of lamellar structure. At the same time, CGCS has a large amount of pozzolanic material and is often used in the manufacture of building materials, ceramics, and other materials. It is worth mentioning that the residual carbon contained in the CGCS is small in quantity, but the disordered carbon crystal structure helps to produce more active sites and improve the adsorption effect.

1.2. Methylene Blue (MB)

Dyestuffs are organic chemicals that may give a colored material a vibrant and firm color. They are diffusely used in industries, including textiles, food processing, and medicines [3]. Approximately 5,000 different dyes are made globally each year, with an annual output of over one million tons. China, as a significant producer and exporter of dyes, produces over 1,200 species annually, with a total yearly output of more than 600,000 tons, exceeding the market demand throughout the country.

There are natural dyes and synthetic dyes, depending on the raw material utilized in

manufacture. Natural dyes are derived from plants and animals and are simpler to decompose and have a lower environmental effect, but the production process is lengthy and costly. This led to the creation of aniline violet, the first synthetic dye, in 1857. More than 7,000 synthetic dyes have been manufactured globally, according to inspection. Synthetic dyes have progressed at a breakneck pace in just a few hundred years. Heavy metals like copper and chromium, which are added to certain dyes, have an increasingly negative influence on the environment and can cause substantial water contamination in particular [4]. As a result, the European Union prohibited chromium mordant dyes in 2002 and limited the use of heavy metal complex dyes comprising copper, chromium, and nickel.

In the field of environmental engineering, dyes are classed as anionic, cationic, or non–ionic based on the ionic form in which the dye molecule dissociates in an aqueous solution. Many of them contain nitrogen–containing groups or anthraquinones, in which the nitrogen bond in the nitrogen–containing group is easily broken when reduced to toxic amines, whereas the aromatic structure in anthraquinones is difficult to degrade, making wastewater decolorization a major issue. During the dyeing process, the vast majority of inorganic substances and a small proportion of organic substances enter the wastewater, constituting a complex of polluting components [5]. In short, the following are the main characteristics of dye wastewater: 1) organic dyes have an aromatic structure, are difficult to degrade, and are highly polluting; 2) the dark color of dye make it resistant to photolysis and oxidation, thus increasing the difficulty of water treatment; 3) dyes can absorb light, reduce the transparency of the water, consume a large amount of oxygen in the water, causing hypoxia, affecting the growth of aquatic organisms and microorganisms, and destroying the self–purification of the water, while

easily causing visual pollution.

Methylene blue (MB) is a cationic dye with a wide range of applications. It can also be employed in the medical field, in addition to being used as a dye in the industry. Figure 1.2 shows the molecular structure of MB. The first application of methylene blue in the treatment of bacterial malaria paved the way for the use of synthetic dye compounds in the treatment of the disease. At the same time, the proper concentration of methylene blue may be employed as a disinfectant in aquaculture, inactivating microorganisms and creating a disinfection effect.
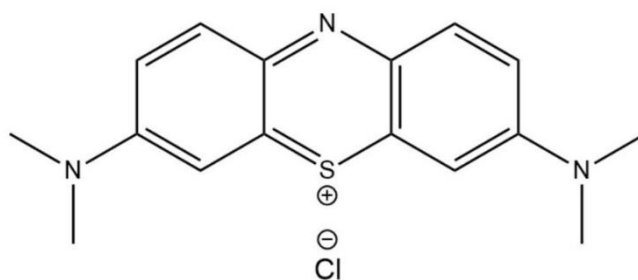
Figure 1.2 Molecular structure of MB.

Methylene blue is an aromatic heterocyclic chemical that must be kept out of direct sunlight. Water, ethanol, and chloroform can all be used to dissolve it. Zinc powder or weak sulfuric acid can be added to an aqueous solution for a reversible fading process and is commonly used for dyeing. Even though methylene blue cures nitrite, cyanide, and other poisonings, it is nonetheless dangerous, irritating to the eyes and skin, and very combustible. According to data, more than 400,000 tons of textile dyes are manufactured globally [6]. According to the guidelines of China Environmental Bulletin, 2020, up to 10 mg/L of dye effluent can be emitted, and 85% of the dye will be released in the dyeing process, causing pollution. According to preliminary data, the national annual printing and dyeing wastewater discharge is 7.2×10^8 m^3 [7].

Methylene blue is an antioxidant reducer that is extremely stable in air. It dissolves in water, ethanol, and chloroform but not in ether. When exposed to more than 500 mg/kg of methylene blue, individuals may experience nausea, dizziness, and chest pain. Methylene blue's toxicity to many aquatic creatures varies and can kill an enormous number of animals when a certain concentration is achieved. Because the food chain is characterized by rising degrees of toxicity, people at the top of the food chain face a massive threat. On the other hand, methylene blue has a blue color when dissolved in water and can diminish the clarity of the water at large concentrations, making photosynthesis difficult for aquatic plants and complicating water treatment. The absence of oxygen degrades the water body's quality, inhibits photosynthesis, and stops organisms from growing normally. Synthetic dyes that include aromatic and heterocyclic compounds are also carcinogenic, and dye wastewater contains prominent levels of metals and other contaminants that can harm plants and animals that come into touch with them.

Up to now, treatment methods for methylene blue–based dyes include biological enzymatic photodegradation reaction, electrochemical method, ultrafiltration, and physical adsorption, among others [8]. Adsorption method with the straightforward process, low cost, and no secondary pollution advantages has become one of the most popular research methods. There are several methods for removing methylene blue by using gasification slag, including zeolites, mesoporous silica, carbon–silicon composite materials, and other porous materials.

1.3. MB Adsorption Mechanism Using Carbon–silicon Composite

Coal gasification slag contains a large amount of SiO_2, Al_2O_3, Fe_2O_3, residual carbon, and other oxides, which can be used to make carbon–silicon composites. The adsorption process of mesoporous silica results in the presence of different forms of silica hydroxyl groups, which are surface–active groups. This structure is able to combine with MB^+ to achieve the adsorption effect. L.T. Zhuravlev [9] suggests that surface silica hydroxyl groups can be divided into four categories: (a) isolated silanol groups, $= SiOH$; (b) genimal silanol groups $= Si(OH)_2$; (c) contiguous silanol groups (containing hydrogen bonds) and (d) siloxane bridges (shown in Figure 1.3).
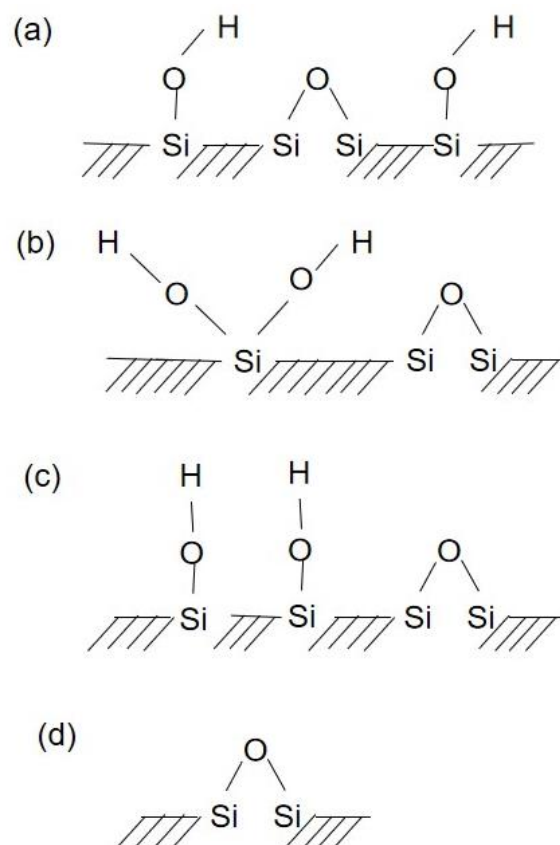
Figure 1. 3 Four kinds of surface–active groups: (a) isolated silanol groups; (b) genimal groups; (c) contiguous silanol groups;(d) siloxane bridge [9].

The influence of these four surface silica structures on adsorption is significant. When the three structures (a), (b), and (c) is present in the solution, they are able to bind well to the methylene blue solution. The two silica hydroxyl groups, (a) and (b), which are connected by a siloxane bridge, lose H^+ in the solution and form free $[SiO]^-$, which binds to MB^+ through electrostatic interactions to achieve adsorption of the pollutant [10, 11]. Figure 1.3 (b), in which one Si atom is connected to two hydroxyl groups, and is able to bind more MB^+, making the removal capacity stronger. Figure 1.3 (c), the main mode of adsorption is the silanol group binding to the N atom on the benzene ring in the methylene blue structure to form a hydrogen bond. The N atom is bonded to a hydrogen bond. In the case of the fine slag–based modified carbon–silicon composites, the formation of hydrogen bonds is less frequent, and electrostatic adsorption is the main mode of adsorption.

Steps such as acid leaching, calcination, and activation are necessary. The residual carbon is converted into activated carbon by elevated temperature activation, which can effectively increase the BET surface area and removal capacity. Furthermore, the relevant substances contained in the minerals in coal gasification slag are converted into amorphous silica structures for the adsorption reaction. When compared to the original technique of eliminating residual carbon, carbon–silicon composites may enhance the BET surface area and the number of surface–active groups of the material in all respects, resulting in a higher removal capacity.

There are six possible adsorption processes in solid adsorption, namely electrostatic interactions, ion exchange, ionic dipole interactions, surface metal cation coordination, hydrogen bonding, and hydrophobic interactions, which are closely related to the

surface properties of the material.
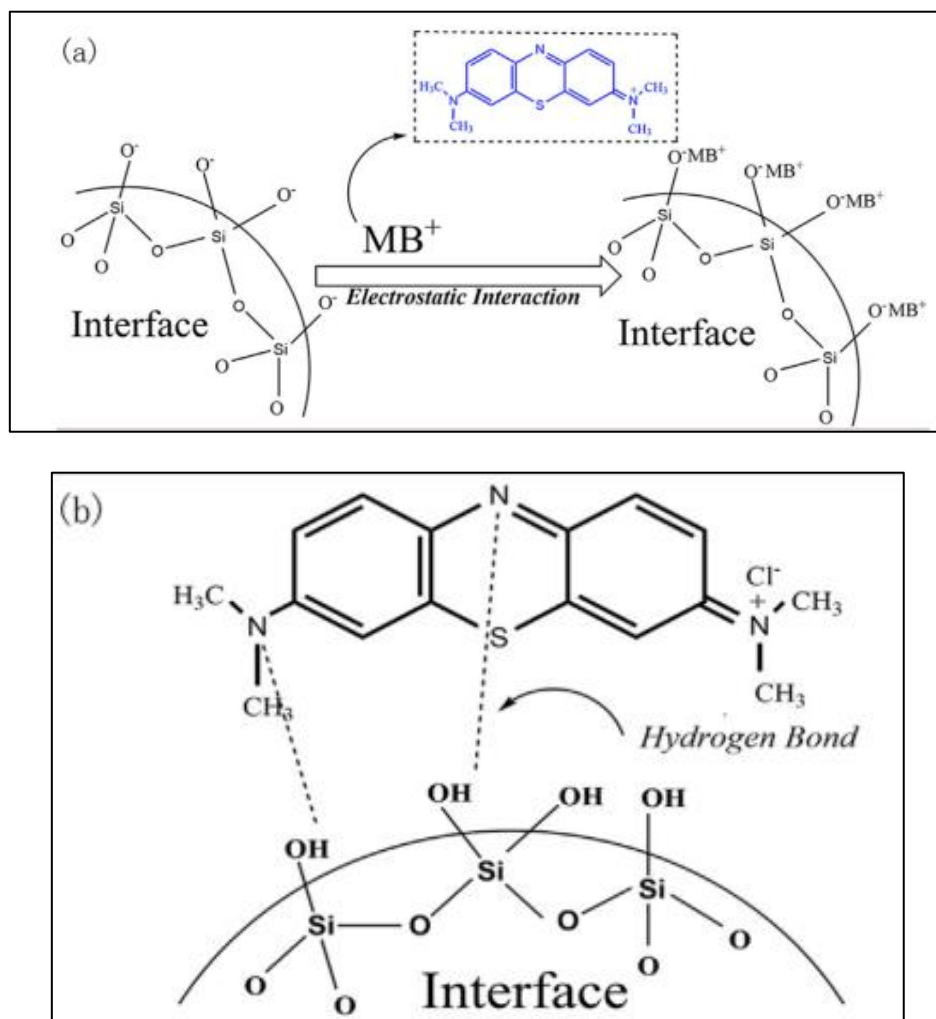
Figure 1. 4 Mechanisms of methylene blue adsorption, (a) Electrostatic Interaction; (b) Hydrogen Bond [9].

Electrostatic interactions were found as the key function of mesoporous silica materials in the adsorption of methylene blue solutions by Liu et al. in their investigation [9]. It is possible for the MB^+ in solution to establish an electrostatic attraction when the silanol surface group in mesoporous silica separates H^+ to make a $[SiO]^-$ structure[10, 11]. Because methylene blue is a cationic dye, it is not surprising that increasing the pH causes more negative charges on the material's surface, which aids MB^+ attraction and increases the quantity of methylene blue adsorbed. He also found that when the reaction

was conducted under acidic conditions, the material still exhibited superior adsorption properties, probably due to the silanol group binding to the nitrogen atoms on the MB and forming hydrogen bonds. Figure 1.4 shows the authors' conclusion that the adsorption of MB by mesoporous silica glass microspheres is an electrostatic and hydrogen bonding process.

1.4. Research Aim

The environmental pressure from industrial wastewater is rising day by day due to the rapid expansion of the printing and dyeing industry. On the other hand, as solid waste, gasification furnace slag may play a positive role in the treatment of industrial wastewater, which can not only mitigate the environmental hazard caused by the organic pollutants and heavy metals but also reuse the CGCS.

There are a number of studies where adsorbents based on modified gasification slag may successfully adsorb organic pollutants and heavy metals. However, their main focus is on the coal gasification fine slag. Because of some of the previously mentioned properties, fine slag has some advantages in the preparation of mesoporous materials. For example, the higher amount of residual carbon contained in the fine slag can be activated to obtain materials with a larger BET surface area [9]. However, in practice, these residual carbons need to be activated by a combination of high concentration of alkali solution and high calcination temperature (over 700 °C) [9]. This increases the energy consumption in the reaction process and has many negative environmental impacts.

Consequently, the aim of this study is to develop a low energy consumption modification approach to convert CGCS into an efficient MB adsorbent. Figure 1.5 illustrates the technology route of this study.
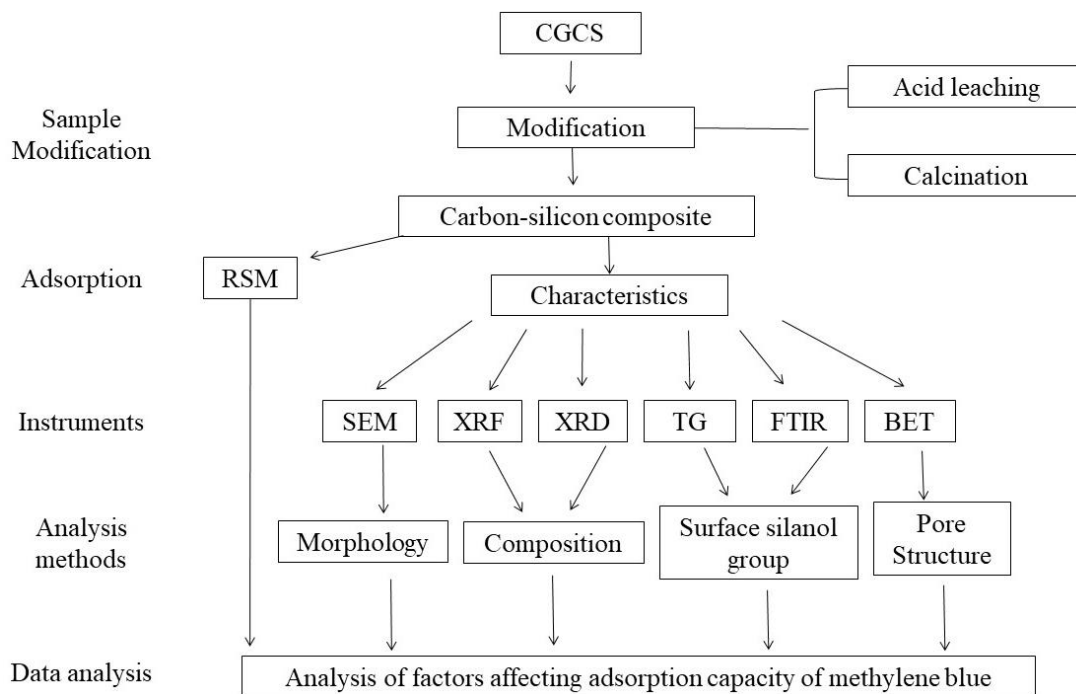
Figure 1. 5 Technical route of this study

2. LITERATURE REVIEW

2.1. Application of Coal Gasification Slag

At the present, coal gasification slag is mostly treated through landfills and stacking. This type of treatment procedure readily allows heavy metals to penetrate the soil, which not only harms the environment but also raises the land occupancy rate, which is highly undesirable. As a result, several studies seek to employ coal gasification slag to alleviate the burden of energy waste [13]. For example, using the natural qualities of coal gasification slag to mix with concrete or as an additive to cement is a direct utilization [14]. The other option is to change the structure of coal gasification slag to create new materials with properties and high added value, such as zeolite and Si–Al–O–N powder [15, 16].
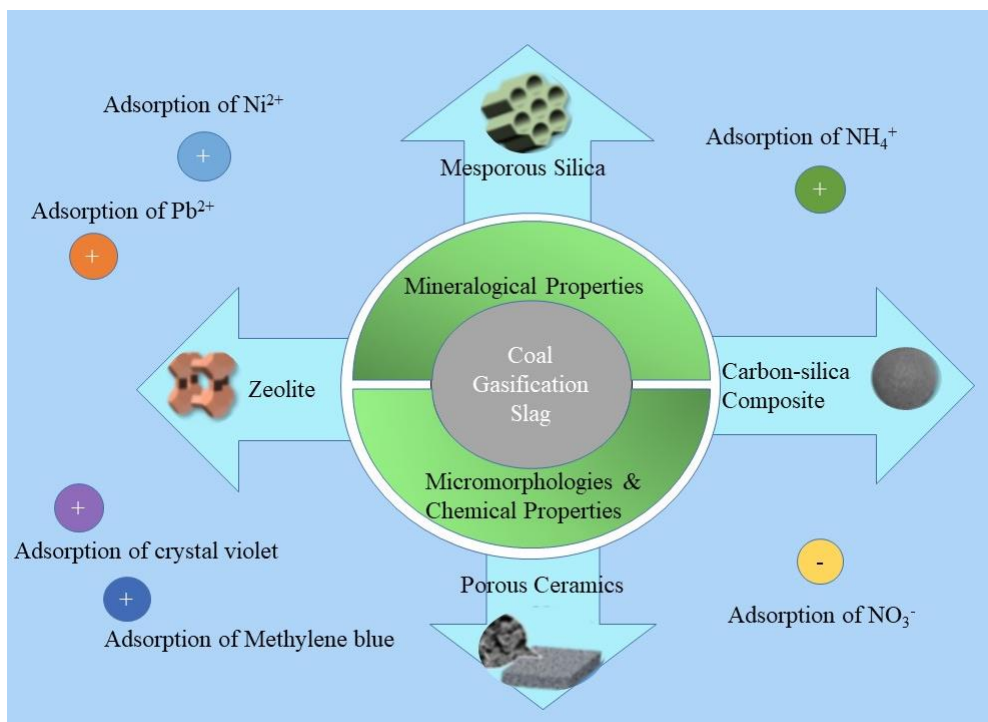
Figure 2. 1 Diagram of coal gasification slag generation production process [17].

Figure 2.1 indicated several methods for modifying coal gasification slag, particularly

for the manufacture of adsorbents via modification. Because it has high pozzolanic activity and contains a high concentration of silica, alumina, and ferric oxide, these properties aid in the preparation of porous materials with rich pore structure and high BET surface area, opening the possibility of porous material preparation. A porous substance is a material that has a network of interpenetrating or closed pores. Increased human activities continue to exert a significant strain on water supplies as urbanization and industrialization progress. Adsorption is currently one of the most numerous methods for treating wastewater pollution, with the advantages of simplicity and efficiency [17, 18].

Table 2. 1 Research about adsorbing organic dyes and heavy metals

Material	Adsorbate	BET surface area (m^2/g)	Removal capacity (mg/g)	Refs.
MCM–41	Crystal violet	1347	635	[19]
Mesoporous silica	MB	364	141	[9]
Carbon–silicon composite	MB	500	182	[9]
Carbon–$CoFe_2O_4$	MB	463	120	[20]
Activated carbon/iron	phenol		117	
oxide magnetic	chlorobenzene	658	305	[21]
composites	chloroform		710	
Carbon–Fe^{3+}	Methyl orange		243	[22]
Carbon/X zeolites	MB	295	93.9	[23]

When gasification slag is utilized as a raw material in the preparation of adsorbent, it is often employed to adsorb two types of contaminants. One is organic dyes, especially

methylene blue and methylene orange. Most of these dyes are produced in printing and dyeing enterprises. The makeup of dyes is complicated; the alkalinity is high, making it tough to decompose. If not handled properly, it will disrupt the ecological balance and create major water pollution. When choosing an adsorption technique, it is possible to achieve high removal efficiency while avoiding secondary pollutants [24]. Adsorption of heavy metals is the other option. Heavy metals, such as mercury, lead, arsenic, and uranium, are primarily obtained by electroplating, mining, battery production, printing, and smelting [25, 26]. Because these contaminants pose a significant danger and have a slow rate of degradation, it is critical to perform effective separation and removal. Table 2.1 listed research using modified coal gasification slag to reduce environmental pollution.

2.2. Porous Materials and Mechanisms

2.2.1 Zeolites

Zeolite, a boiling stone, is a natural aluminosilicate mineral that boils when heated. Scientists created artificial zeolite by emulating the natural zeolites' time–consuming creation conditions. Silicon, aluminum, and phosphorus atoms form a TO4 tetrahedral skeleton with shared vertices [27]. Depending on the composition, zeolites can have different properties such as ion exchange, adsorption, and catalytic activity [28, 29]. To date, the conversion of coal gasification slag has resulted in the successful construction of zeolites P and X [16].

To manufacture zeolite P, the process is shown in Figure 2.2. The amorphous silicon

and alumina in coal gasification slag are used as a source of silica–aluminum, which is then prepared by mixing the coarse residue with sodium hydroxide [16]. This approach not only makes use of the slag's characteristics but also stabilizes the structure of zeolite by adding Na^+ [7]. Furthermore, a sufficient number of –OH groups might improve amorphous gel breakdown, minimize the induction time, and speed up the crystal formation [30].
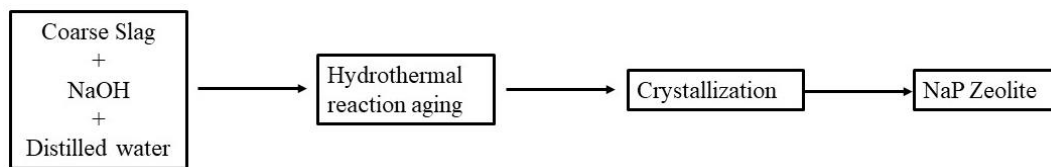
Figure 2. 2 Schematic diagram of the preparation process [17].

Zhang et al. (2018a) produced zeolite X using two methods: alkali melting [31] and hydrothermal synthesis [7]. The addition of NaOH can aid the reaction, and the alkali fusion technique activated soluble silicate and aluminate reaction can, to some extent, increase the pore size and BET surface area as well as the MB adsorption capacity (93.9 mg/g) [32]. The principle of zeolite preparation is to use amorphous silica and alumina in the gasification slag, followed by a NaOH reaction, to prepare a stable tetrahedral structure by the hydrothermal method. At the same time, this preparation method increases the BET surface area of the zeolite, which eases the removal of pollutants.

2.2.2 Mesoporous Silica

The first successful preparation of porous silica was in 1995 when researchers used sol–gel technology to successfully construct a molecular skeleton of porous silica using ordered supramolecular micelles prepared from surfactants as a template [33]. This

approach, like zeolite synthesis, employs coal gasification slag as a silicon aluminum source for activation and extraction. Acid leaching, alkali melting, and high-temperature calcination are common pretreatment procedures that can convert crystalline mullite into an acid–soluble nepheline phase [34].

Many investigations are being conducted based on the findings of zeolite research, with the goal of creating a new stable structure, namely, an ordered molecular sieve created highly ordered hexagonal uniform pores by reacting with amorphous phase structure and adding NaOH [35]. Furthermore, Wu et al. (2020) obtained MCM–41 materials with six times larger BET surface area (1013–1073 m^2/g) than synthetic zeolites using hexagonal arrays and one-dimensional channels at 300 $^{\circ}$C [19]. Simultaneously, researchers are beginning to focus on the residual carbon in them, which can either be activated into an activated carbon–like substance or may function as a heat source for the reaction to accelerate it. Also, the researchers used low–temperature calcination of residual carbon, acid leaching, and the P123 template to effectively synthesize Fe–Al–Ti–SBA–15 with a BET surface area of 345–704 m^2/g [27].
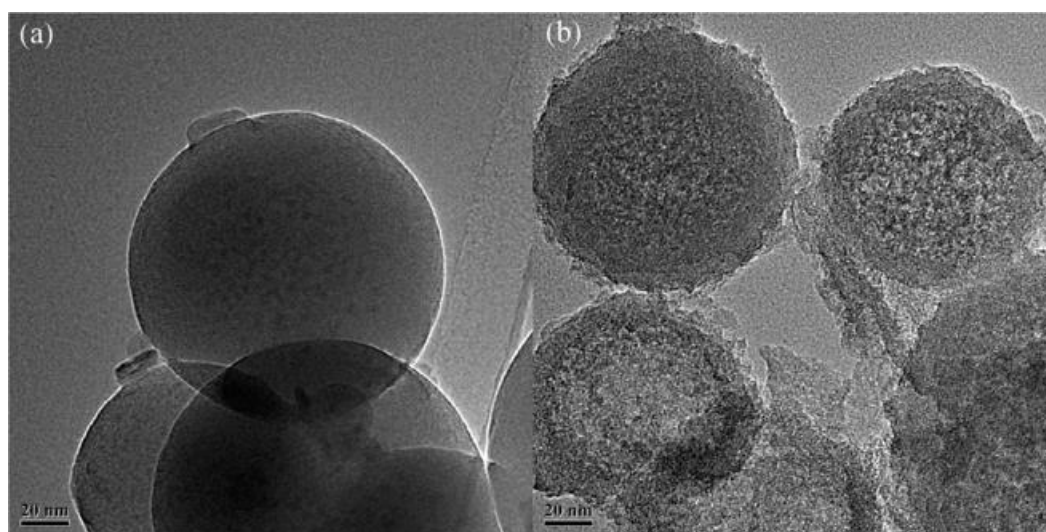
Figure 2. 3 The TEM images of raw material FS1 (a) and mesoporous glass microsphere (b) [14].

In addition to the molecular sieves mentioned above, Liu et al. [9] made mesoporous glass microspheres (mesoporous silicon) by combining fine slag with hydrochloric acid and calcining at high temperatures to eliminate the carbon component. Figure 2.3 shows the TEM structure of mesoporous glass microsphere. This method works by acid leaching the surface metal oxides to form pores and then eliminating the contaminants through the silanol groups created at the surface as shown in Figure 2.4, and MB adsorption capacity of his study is 141 mg/g.
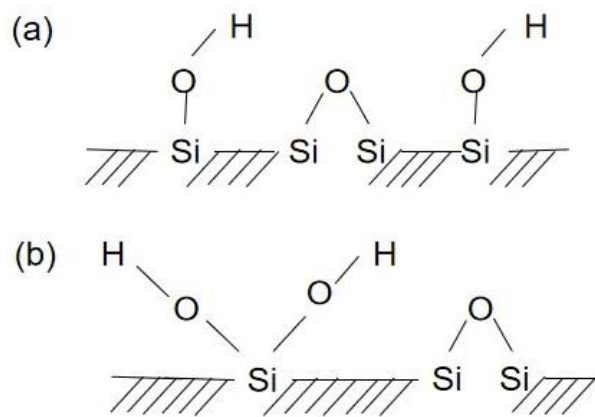
Figure 2. 4 Types of silanol groups and siloxane bridge on the surface of FS1–MGS8. (a) Isolated silanol groups; (b) Genimal silanol groups [14].
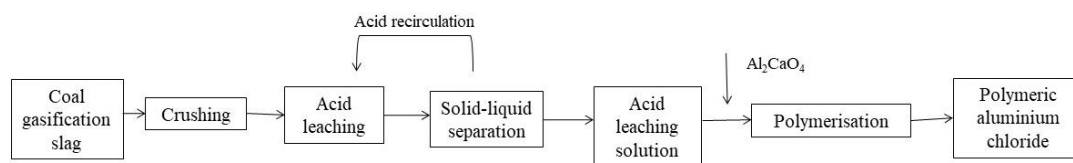
Figure 2. 5 Preparation process of polymeric aluminum chloride from coal gasification slag [36].

Hu et al. [36] prepared polymeric aluminum chloride flocculants by acid leaching for the treatment of water pollution problems (shown in Figure 2.5). The optimum process conditions are the acid concentration of 300 g/L, the reaction time of 120 min, the

reaction temperature of 90 ℃, and the liquid to solid ratio of 5. The reaction time was 120 min, the reaction temperature was 90 ℃ and the liquid to solid ratio was 5. Under these conditions, the alumina leaching rate reached 44.0% and the concentration of aluminum ions in the acid solution reached 28.0 g/L after four cycles.

2.2.3 Carbon−silicon Composite

Residual carbon draws researchers into the study of coal gasification slag because of its good pore structure [37]. The quantity of residual carbon created by various technological processes varies. The researchers determined that the residual carbon in the coal gasification slag could be activated into activated carbon and then mixed with an amorphous silica structure to produce a carbon−silicon composite that adsorbs the dye. As we all know, activated carbon is frequently used as a wastewater adsorbent with varying pore diameters. The macropore as a channel, mesopores operate as channels and adsorption macromolecules, whereas micropores are the primary contributors to adsorption [38]. As a result, the primary goal of this type of approach is to create more pore structures, particularly micropores.

Xu and Chai (2018) activated a KOH−coal gasification slag mixture with a mass ratio of 3:1 at 750 ℃ for 1 h to generate porous carbon [39]. KOH dehydrates and is transformed to K_2CO_3 when the calcination temperature falls below 700 ℃. At 700–750 ℃, K_2CO_3 dissolved into CO_2 and K_2O, and the K_2O and K_2CO_3 subsequently diffused through the carbon network, where they were reduced to metal K by carbon [40, 41]. Metal K penetrates the carbon lattice and is removed during the secondary pickling process, resulting in irreversible lattice network expansion and the creation of high

porosity. At this point, the microporous structure was formed. The growth of micropores and the merging of pores happen simultaneously at 750–800 ℃ [42]. The optimal sample had a BET surface area of 2481 m^2/g on the BET scale, and the carbon–enriched composites were highly hydrophobic. Figure 2.6 depict this pore configuration.
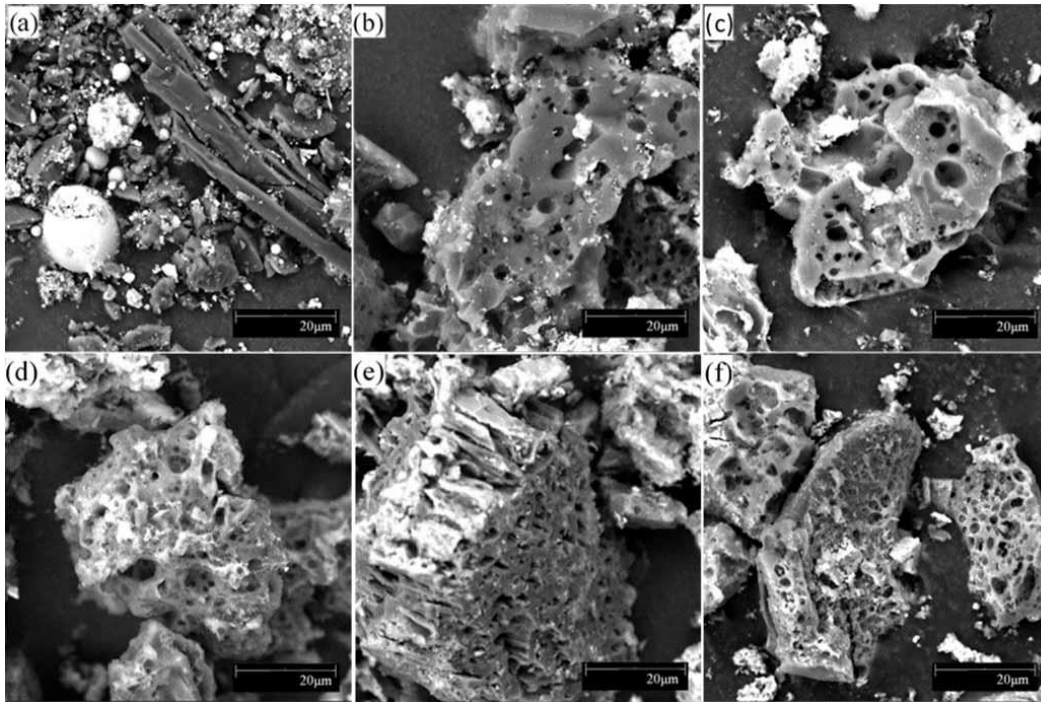
Figure 2. 6 Surface morphology of coal gasification slag [43].

Homoplastically, Gu and Qiao (2019) used KOH to produce carbon-silicon composites from gasification fine slag [43]. KOH interacted with carbon in coal during alkali melting to produce K_2CO_3, K_2O, H_2, and CO. Complete volatilization of metal K from coal at 1047 K, causing K_2CO_3 and K_2O to react with C at the same time. Micropores were generated in both processes, and residual carbon was transformed into graphite C [40, 41]. Then, along with the graphite C and SiO_2 created narrow slit–shaped mesopores during the following acid leaching step, in which hydrochloric acid dissolved $KAlO_2$, Al, and Fe to form mesopores, resulting in increased porosity.

Furthermore, coal gasification slag can also generate dendritic mesoporous channels by removing randomly dispersed metal oxides by direct acid leaching [9]. Zhu et al. used a hydrochloric acid leaching experiment on fine slag to create carbon–silicon mesoporous composites [44]. In this image, the creation of amorphous silica glass microspheres in a hydrochloric acid solution is demonstrated. The oxides in the fine slag are gradually dissolved by the hydrochloric acid solution, producing uneven channels. The generated channels may join with one another during the process to produce bigger mesoporous channels. The following are the hydrochloric acid leaching reaction equations for metal oxides:

$$Al_2O_3 \cdot SiO_2 + 6H^+ = 2Al^{3+} + 3H_2O + SiO_2 \tag{1}$$

$$Ca_2SiO_4 + 4H^+ = 2Ca^{2+} + H_4SiO_4 \tag{2}$$
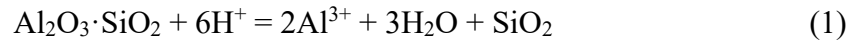
In summary, carbon–silicon composites exhibit high hydrothermal and chemical stability and may be widely used as an adsorbent [45-49].

3. EXPERIMENTAL

3.1. MB Adsorption Using CGCS-CSC

3.1.1. Materials and Chemicals

Rongxin coal gasification coarse slag is obtained from Inner Mongolia Rongxin Chemical Co., Ltd. The ball milling method can efficiently grind large particle samples and CGCS–BM is the sample after ball milling. Figure 3.1 shows CGCS and CGCS–BM samples. In this study, a 200–mesh sieve was selected to make CGCS–BM particle size < 100 μm, which can increase the contact area during the reaction, especially for the acid leaching process. The chemical compositions of Rongxin coarse slag are shown in Table 3.1. Table 3.2 shows the information of chemicals used in the experiments.

Table 3. 1 Inductively coupled plasma (ICP) test of Rongxin coarse slag

	Si	Ca	Fe	Al	Na	K	S	Mg
Rongxin Coarse Slag (%)	7.21	6.12	3.63	3.58	0.859	0.383	0.264	0.202

Figure 3. 1 Samples of CGCS (left); CGCS–BM (right).

Table 3. 2 Information of Chemicals used in the experiments

Reagent name	Purity	Manufacturer	Solution preparation
Hydrochloric Acid (HCl)	AR	Sinopharm Chemical Reagent Co., Ltd	Measure 10.8, 21.6, 32.4, 43.2, 54.1 mL of concentrated HCl, add water to 100 mL, to prepare 4, 8, 12, 16, 20 wt% HCl
Potassium Hydroxide (KOH)	AR	Sinopharm Chemical Reagent Co., Ltd	Sample: KOH =1:3 (weight ratio), mix well under aqueous solution
Acetic Acid (HAc)	AR	Sinopharm Chemical Reagent Co., Ltd	Measure 16.3, 20.4 mL HAc to prepare 16, 20 wt% HAc
Methylene Blue (MB)	AR	Sinopharm Chemical Reagent Co., Ltd	Prepare 85–115 mg/L and 100–300 mg/L Methylene blue

3.1.2. Response Surface Methodology

Response surface methodology (RSM) is one of the most important branches of experimental design. It is used to assess the impact of several variables and their interactions on the system's response. It is a blend of mathematics and statistical techniques. This strategy is very good for creating and optimizing independent variables and responses as well as reducing experimental runs compared to traditional

methods. In recent years, efforts to better understand adsorption processes and the impacts of various parameters on adsorption behavior have been enhanced [34, 35]. It is most commonly used in situations where a large number of variables influence the system response [6, 34, 39]. It consists of three phases, as stated previously: Experiment planning; Modeling, and optimization of response surfaces [6]. This study chose the Central Composite Face methodology for the experimental design.

3.1.3. Concentration of MB

MB reserve solution configuration: 1 g methylene blue, dissolved in 1 L deionized water, prepared into 1g /L reserve solution, and put in a brown reagent bottle for later use. During the experiment, it was diluted to five concentration gradients of 100−500 mg/L. In this study, UV−VIS was chosen to determine the change in the concentration of MB as shown in Figure 3.2.

Figure 3. 2 The image of UV−VIS.

Spectrophotometry is a qualitative and quantitative analysis method based on the Lambert-Beer law for substances with characteristic absorption peaks in the UV−visible

region [50]. Due to the difference in composition and structure of different substances, the molecular vibration and electron energy level transition after absorption of light energy are different, that is, the absorption spectrum curves of substances are different. Therefore, the content of a substance is usually determined by the absorbance of the substance at the characteristic wavelength.

In this method, attention should be paid to: (1) The absorbance of MB with different concentration gradients should be measured before the experiment, to draw a standard curve; (2) Ensure the correct use of colorimetry. Quartz colorimetry is used to determine the wavelength range of 200–350 nm in the ultraviolet region of the material, glass colorimetry is used to determine 350–100 nm in the visible region of the material [51, 52].

3.1.4. Synthesis of CGCS-CSC

The samples for the experiments were prepared as follows: 100 g CGCS was completely dried in an oven at 120 ℃. Weigh the agate ball–sample weight ratio of 10:1 and ball mill at room temperature for 10 minutes. After ball milling, the sample was obtained through a 200–mesh sieve. CGCS–BM was prepared.

Then weigh 10 g CGCS–BM and mix it with 16 wt% HCl at the ratio of 1 g: 20 mL. Stir it at room temperature for 3 h. After acid leaching, filter and wash the solids to neutral, and dry them in the oven at 120 ℃ overnight. The dried sample and KOH were mixed in an aqueous solution with a weight ratio of 1:3. To prevent boiling, the mixed solution should be dried in an oven before calcined at 550 ℃ for 2 h, then washed with

hot water for 1 h. After cooling, filtered, washed to neutral, and dried overnight at 120 ºC to obtain CGCS–CSC.

3.2. Instrumental Characterizations of CGCS-CSC

3.2.1. Scanning Electron Microscope (SEM)

Scanning electron microscope (SEM) is widely utilized to examine the morphological structure, interface conditions, damage processes of diverse materials (shown in Figure 3.3). To improve the electrical conductivity and viscosity ability, the sample was coated with gold for a thickness of about 10 nm [21].

Figure 3. 3 SEM gold spraying equipment (left) and test machines (right).

3.2.2. X-Ray Fluorescence (XRF)

Figure 3.4 shows X–ray fluorescence (XRF) test equipment and tablet press machine. Weigh 2–5 g of CGCS–CSC solid powder and dry it overnight at 120 ºC. The powder was placed in a plastic ring and crushed into sample pieces under 600 kN pressure for 1 minute [53].

Figure 3. 4 XRF test equipment (left) and tablet press machine (right).

3.2.3. X-ray Diffraction (XRD)

X–ray diffraction (XRD) employs monochromatic X–rays as a diffraction source, which can typically penetrate a solid and to verify its interior structure, providing information on the material's bulk structure. To perform the XRD test, firstly, weigh about 1 g of the sample and place it on the sample table so that the sample fills the center of the sample table evenly and adequately. The XRD test is then performed according to the following conditions: 10–80°, 0.02°/step, 2 s/step, 40 kV, 40 mA. Figure 3.5 shows the XRD equipment and prepared samples.

Figure 3. 5 The images of XRD and samples prepared.

3.2.4. Brunner–Emmet–Teller (BET)

The Brunner–Emmet–Teller (BET) equation may be used to calculate the BET surface area of non-porous, microporous, and mesoporous materials [54]. Studies show that the pressure range of single/multilayer adsorption on the pore wall is so near to the pressure of condensation in the pore, the BET technique may have some issues assessing mesoporous materials with pore diameters less than 4 nm [55-57]. Figure 3.6 shows the BET test equipment and degas equipment. The preparation procedure of the sample for BET measurement is described as follows: weigh the empty tube + stopper as m_1; weigh 0.5 g of the dried sample into the tube and weigh the sample + tube + stopper as m_2; perform degas at 300 ºC for 6 h. After degassing, weigh the tube + stopper + sample as m_3. Subsequently, fill in m_1 and m_3 in the software and select the mesopore method to start the test. Note that the process of degassing is correct when $m_3 \leqslant m_2$. It's worth mentioning that the BET laboratory must keep track of two values: the empty sample and the sample's weight after degassing [9]. Because the BET measurement is so tiny, the margin of error is relatively minimal.

Figure 3. 6 The images of BET, test equipment (left), and degas equipment (right).

3.2.5. Fourier Transform Infrared Spectroscopy (FTIR)

Theoretically, Fourier transform infrared spectroscopy (FTIR) detection is based on the Lambert-Beer law. The FTIR detection principle is depicted in Figure 3.7. The Michelson interferometer's two infrared beams interfere with each other, resulting in interference light I_0 interacting with the sample to be measured in the gas pool [58]. The dipole moment of gas molecule vibration in the gas pool absorbs the typical infrared spectrum, resulting in spectral intensity I of output light attenuation in some bands. The preparation procedure of the sample for FTIR measurement is described as follows: weigh 0.5 g of sample and mix well with 1−2 g of KBr and pour into the mold. Press the mold into the tablet press at 10 MPa pressure for 3 minutes. When removed, the sample is a translucent sheet, which makes it easy for different wavelengths of infrared light to pass through the sample and get different peak curves to analyze.
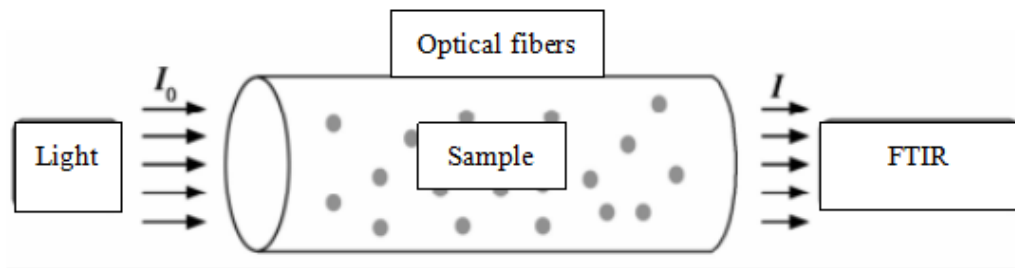
Figure 3. 7 The mechanism of FTIR [26]

3.2.6. Thermogravimetric Analysis (TGA)

Thermogravimetric Analysis (TGA) is the study of a specimen's significant change in mass throughout the heating process. It is used to explore the thermal stability, decomposition processes, dehydration, dissociation, oxidation and reduction, etc. Figure 3.8 shows TGA equipment and sample loading place. The preparation procedure of the sample for TGA measurement is described as follows: weigh 20 mg of dried sample into the crucible and heat up at a rate of 10 °C/min in the temperature range of 180–1100 °C at N_2 atmospheres.
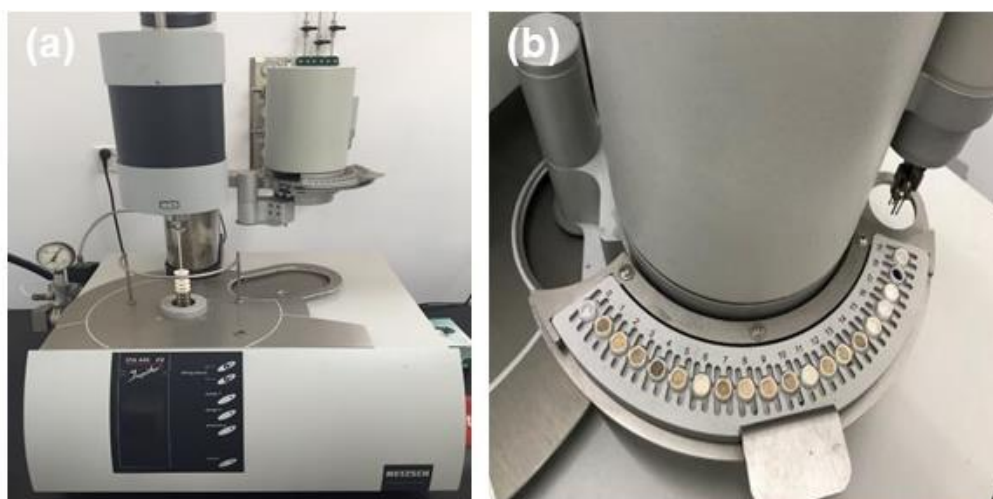
Figure 3. 8 The images of TGA, (a) Test equipment, (b) Sample loading place.

3.3. Adsorption Thermodynamics and Kinetics

3.3.1. Adsorption Isotherm

In a constant temperature shaker, the samples were agitated at 150 rpm for 150 minutes. The adsorbed samples were filtered, and the methylene blue concentration was measured spectrophotometrically. The removal capacity is determined using the equation [9] below:

$$q = \frac{(C_0 - C_e) \times kV}{m} \tag{3}$$

Where k represents dilution ratio, V is the volume of solution at the reaction time, m denotes the quantity of CGCS–CSC added and C_e and C_0 denote the subsequent and pre-sorption concentrations, respectively.

3.3.2. Adsorption Kinetics

Measure 100 mL of MB solution, add 0.05 g of CGCS–CSC, and mix for 250 min at room temperature at 150 rpm. The solution was measured for different adsorption periods, measured in about 3 mL, and its absorbance was determined by UV spectrophotometry, and then the concentration of MB was calculated by the standard curve.

4. CHARACTERISTICS OF CGCS–CSC

4.1. Microstructure

The acid concentration was discovered to be the most crucial component affecting the pore structure. Using CGCS as raw material, the influence of different concentrations and types of acids on the pore structure was examined. Figure 4.1 shows curve e, which represents CGCS–BM, processed by mechanical ball milling. It has a BET surface area of 116 m^2/g. The effect of different concentrations of hydrochloric acid (HCl) and acetic acid (HAc) on the BET surface area of the samples following acid leaching is represented by curves a–d.
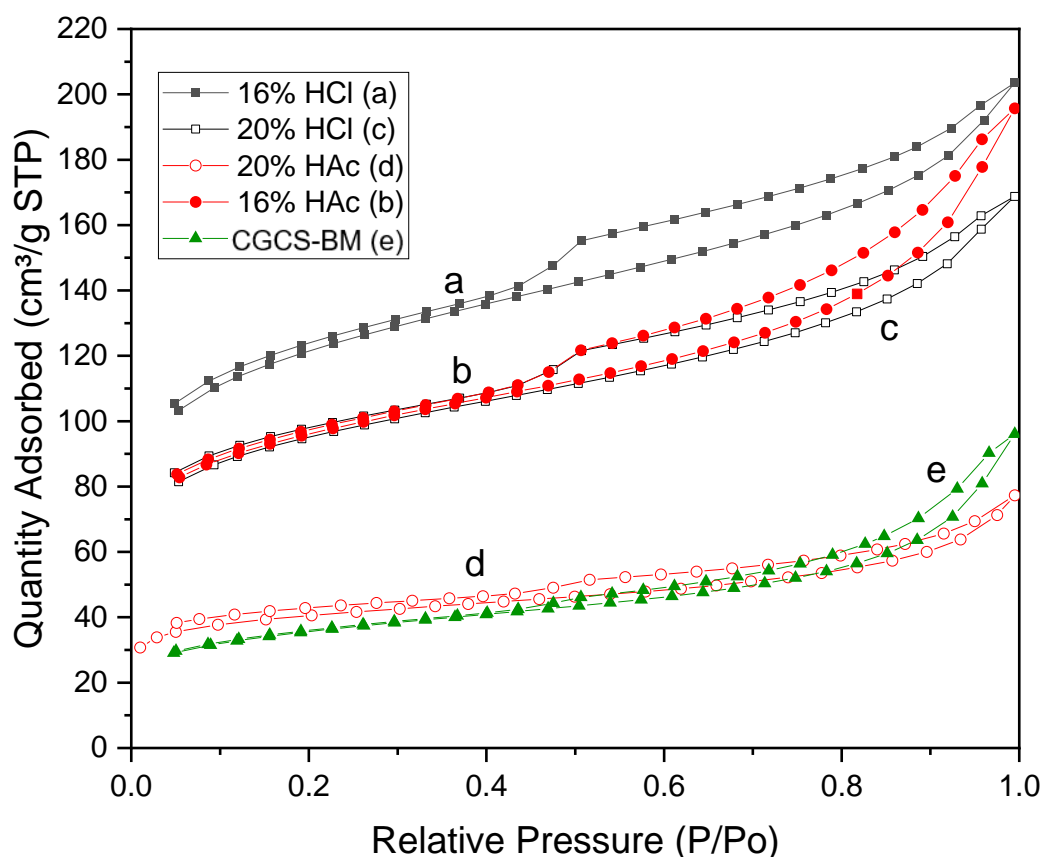
Figure 4. 1 Adsorption/desorption curves of acids at different concentrations: (a) 16 wt% HCl, (b) 16 wt% HAc; (c) 20 wt% HCl; (d) 20 wt% HAc; (e) CGCS–BM

The pore characteristics of CGCS–CSC generated at various acid concentrations are shown in Table 4.1. BET surface areas and trend changes varied amongst acid species. Both HCl and HAc can effectively raise the BET surface area of CGCS. However, their characteristics are quite different. The BET surface area fell from 394 to 308 m^2/g when the HCl concentration rose. It increased from 311 to 373 m^2/g while the HAc concentration increased. This means that in a certain concentration range, the BET surface area is inversely proportional to HCl but positively correlated with HAc.

Table 4. 1 Effects of different concentrations of acid on BET surface area

Concentration (wt%)	Acid	BET surface area (m^2/g)
0	/	116
16	HCl	394
20	HCl	308
16	HAc	311
20	HAc	373

When comparing curve a and curve b, the BET surface area after 16 wt% HCl treatment was 84 m^2/g larger than that after the same concentration of HAc treatment, indicating that HCl has a stronger ability to build pore structures than HAc at low concentrations. This may be because the low concentration of HCl can leach out the metal oxides from CGCS–BM more slowly and effectively without incomplete reaction due to too low concentration.

Comparing curve b and curve d, the quantity adsorbed of HAc falls from 80 to 35 cm^3/g as the concentration rises, and the adsorption–desorption curve in curve d does not

entirely close. This may be due to the small BET surface area of the material or the presence of unique groups and chemical properties on its surface that prevent complete detachment of the adsorbed gas molecules.

In this thesis, the principle of pore construction is that a certain concentration of HCl leaches metal oxides such as CaO, Fe_2O_3, and Al_2O_3 to form pores. The activity of metal oxides has a minor influence on the leaching rate, according to Liu et al. [9], but the concentration of acid is proportional to the leaching rate of metal oxides until saturation is achieved. However, it was discovered in this investigation that a high concentration of acid reduced the BET surface area of the samples, despite the fact that increasing the leaching rate of metal oxides was favorable. When the acid interacts adequately with CGCS–BM, the leaching rate of metal oxides by weak acid is slower than that of a strong acid, which can keep the holes formed during leaching intact. Therefore, the selection of an appropriate concentration of acid is crucial to control the leaching of metal oxides from CGCS. However, because $CaSO_4$ in coarse slag is only weakly soluble in HCl, the sample with the largest BET surface area (394 m^2/g) was chosen for acid leaching studies using 16 wt% HCl.

4.2. Composition

The composition of CGCS–CSC is shown in Table 4.2. CGCS contains many substances such as SiO_2, Al_2O_3, and Fe_2O_3. However, this does not mean that all these substances are present in the form of oxides, especially CaO and Na_2O. They are more unstable and therefore need to be judged by other analytical methods.

Table 4. 2 XRF of Rongxin coarse slag

	SiO$_2$	Al$_2$O$_3$	CaO	Na$_2$O	Fe$_2$O$_3$	MgO	SO$_3$	K$_2$O
Rongxin Coarse Slag (%)	39.1	20.3	15.4	10.3	9.62	2.38	0.791	0.751

During coal gasification, complex phase shifts occur. For example, kaolinite turns into metakaolin before transforming into mullite; quartz transforms into tridymite and cristobalite. These phase changes represent the material changes during the reaction of the substances in the coal gasification slag with the alkaline medium [43]. The relevant reaction equations (4), (5), and (6) are as follows. Preparations are made for the final conversion into a glassy amorphous state at elevated temperatures. The amorphous material utilized in this investigation had a high reactivity, which facilitated metal oxides to leach from it.

$$2KOH + Al_2O_3 = K_2O \cdot Al_2O_3 + H_2O \tag{4}$$

$$2KOH + Al_2O_3 + 2SiO_2 = K_2O \cdot Al_2O_3 \cdot 2SiO_2 + H_2O \tag{5}$$

$$K_2O \cdot Al_2O_3 \cdot 2SiO_2 + 4CaO = K_2O \cdot Al_2O_3 + 2(CaO \cdot SiO_2) \tag{6}$$
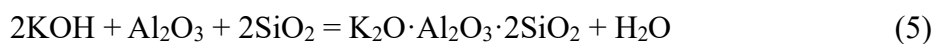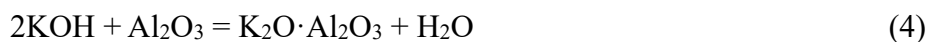
Figure 4.2 shows the XRD spectrum of CGCS−CSC. The high diffraction dispersion indicates that the sample is very disordered. Comparing CGCS−BM and CGCS−CSC, it can be found that the characteristic peak representing SiO$_2$ appears in the modified samples when at $2\theta > 50$ º, indicating the content of amorphous silica (around 58 º) and Al$_2$O$_3$ (around 68 º) in the modified samples increases significantly.

A small amount of HCl reacts with Al$_2$O$_3$ during this process, which leads to a small amount of Al$_2$O$_3$ remaining. This indicates that 16 wt% HCl can leach the metal oxides

in CGCS well. In addition, the sample contains some $CaSO_4$, which can be removed at high temperatures (over 60 °C), but this may lead to solvent evaporation and uncontrollable hazards, so the elevated temperature acid leaching method is not recommended.
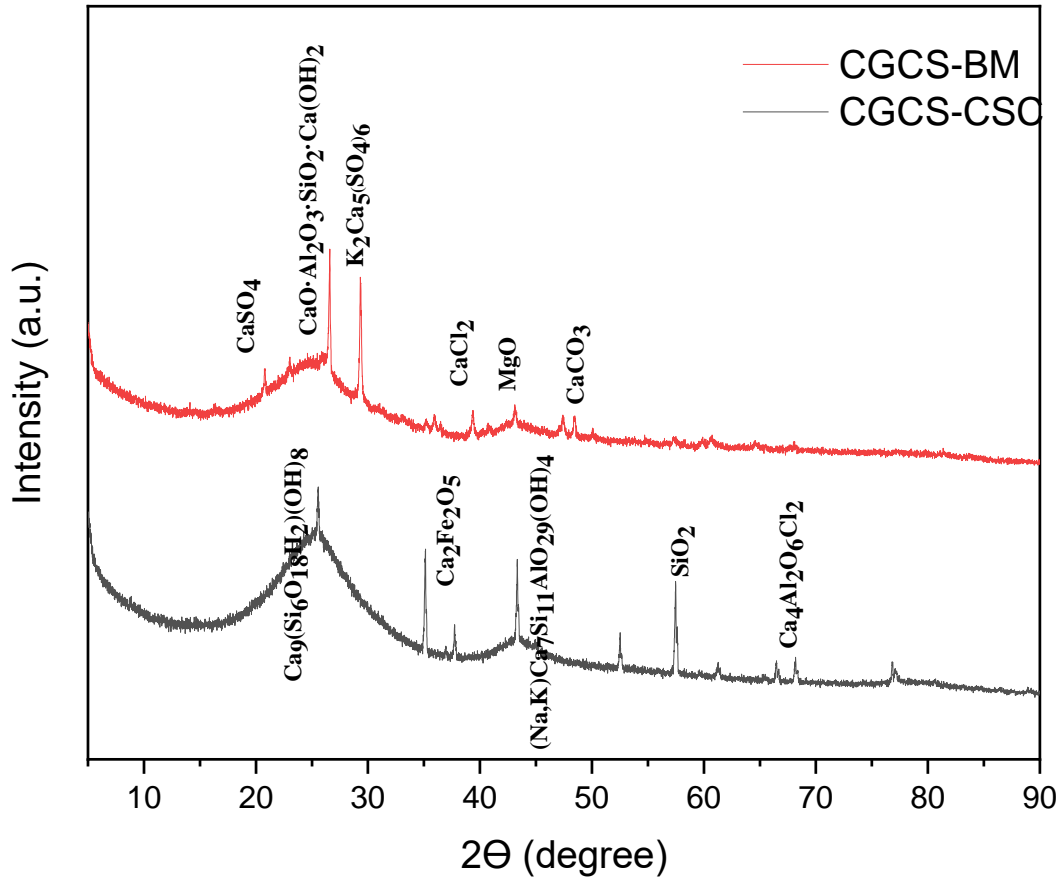
Figure 4. 2 XRD and substance containing

In this thesis, the acid leaching time (3 h) was extended at room temperature to completely leach out the metal oxides, and the solution did not pose a significant environmental hazard, except for the high $CaSO_4$ content.

4.3. Morphology

Figure 4.3 shows scanning electron microscopy (SEM) images of the CGCS–BM and

CGCS–CSC. It can be seen in CGCS–BM under 50.0 μm, in which inorganic minerals and agglomerated residual carbon are interspersed with angular and unevenly sized particles, a small portion of which is bound to the surface by fine glass. The modified CGCS–CSC consists mainly of porous activated carbon structures formed by loosely exfoliated carbon fractions and amorphous mesoporous silica structures. The CGCS–CSC is composed of more fragmented and disordered forms, as well as a highly porous lamellae structure.
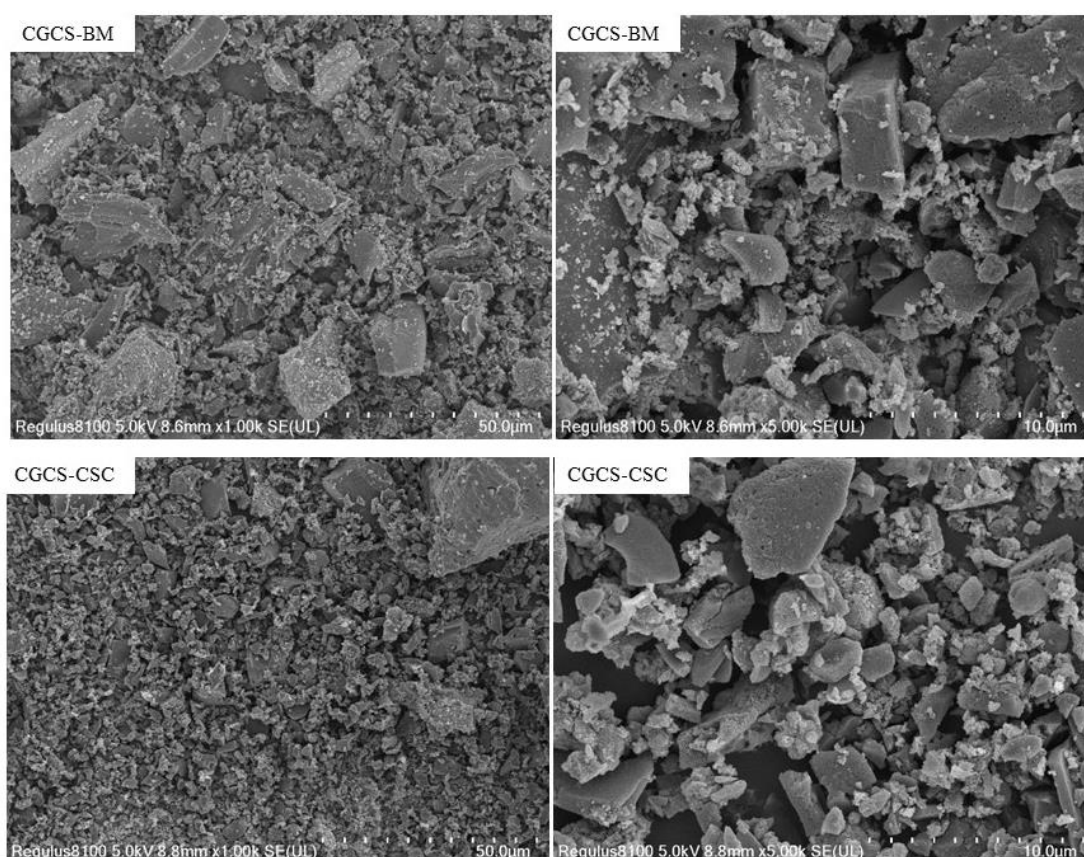
Figure 4. 3 SEM micrographs of CGCS–BM and CGCS–CSC with different magnifications.

Table 4.3 shows EDS of CGCS–BM and CGCS–CSC. The carbon content in CGCS–BM is about 58%, Al is about 10% and Si is about 12%, while the treated CGCS–CSC contains about 47% carbon, 18% Al and 21% Si. This indicates that about

11% of carbon was lost during the preparation process to participate in the activation reaction, and the remaining carbon was activated into mesoporous carbon, and Al and Si elements were produced to form mesoporous silica, which was combined to form a composite mesoporous material for adsorption of MB.

Table 4. 3 EDS of CGCS–BM and CGCS–CSC

	CGCS–BM	CGCS–CSC
C	58%	47%
Si	12%	21%
Al	10%	18%

The TEM images (Figure 4.4) illustrate the formation of mesoporous materials with disordered structures, which may be due to the different morphologies and intermixing of the material components in the samples.
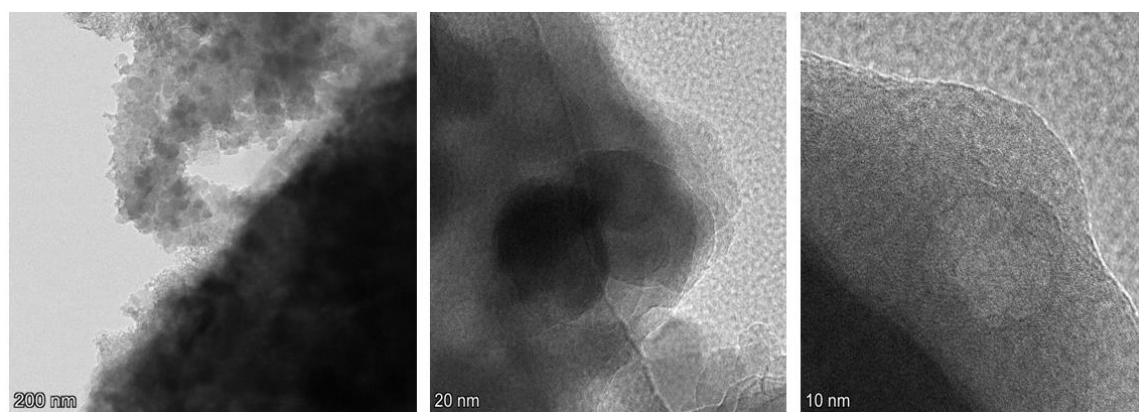
Figure 4. 4 TEM micrographs of CGCS–CSC with different magnifications.

4.4. Silanol Groups

Figure 1.3 shows four kinds of surface silica hydroxyl groups: (a) isolated silanol groups, = SiOH; (b) genimal silanol groups = $Si(OH)_2$; (c) contiguous silanol groups

(containing hydrogen bonds) and (d) siloxane bridges [9]. Table 4.4 indicates the effect of different preparation temperatures on the silanol groups on the surface of the material.

Table 4. 4 The relationship between temperature and −OH type content

Temperature (ºC)	< 25	25–190	190–400	400–900	900–1200
─OH Content	a, b, c	a, b, c	a, b	a	d

When the calcination temperature exceeds 900 ºC, there are no groups in the system that can bind to MB, which stipulates that the calcination temperature must be less than this value to ensure that the adsorption reaction proceeds smoothly. Some methods of modification with fine residues require heating to 800 ºC to achieve K removal [42]. Because the reaction of K^+ with other substances is made possible by substitution to give metal K, which has a volatility temperature of about 774 ºC, the heating to 800 ºC causes K to volatilize and a pore to form where K would otherwise be, increasing the BET surface area to 1347 m^2/g [42]. At this time, most of the silanol groups are isolated silanol groups, and such adsorption is based on electrostatic interaction. If the adsorption is to be increased effectively, more reactive silanol groups should be constructed within the system, and this can be attempted by appropriately lowering the calcination temperature. Therefore, the MB adsorption of CGCS–CSC was tested at three calcination temperatures (shown in Table 4.5), 450, 550, and 650 ºC [59]. It was found that the BET surface area was maximum at 550 ºC when both isolated silanol groups and genimal silanol groups should be present in the system.

Table 4. 5 Different BET surface areas under 450–650 ºC

Calcination temperature (ºC)	BET surface area (m^2/g)
450	255
550	438
650	406

To determine the type of silanol groups within the system and the reaction mechanism, FTIR tests were performed. Figure 4.5 shows the FTIR spectrum of CGCS–CSC.
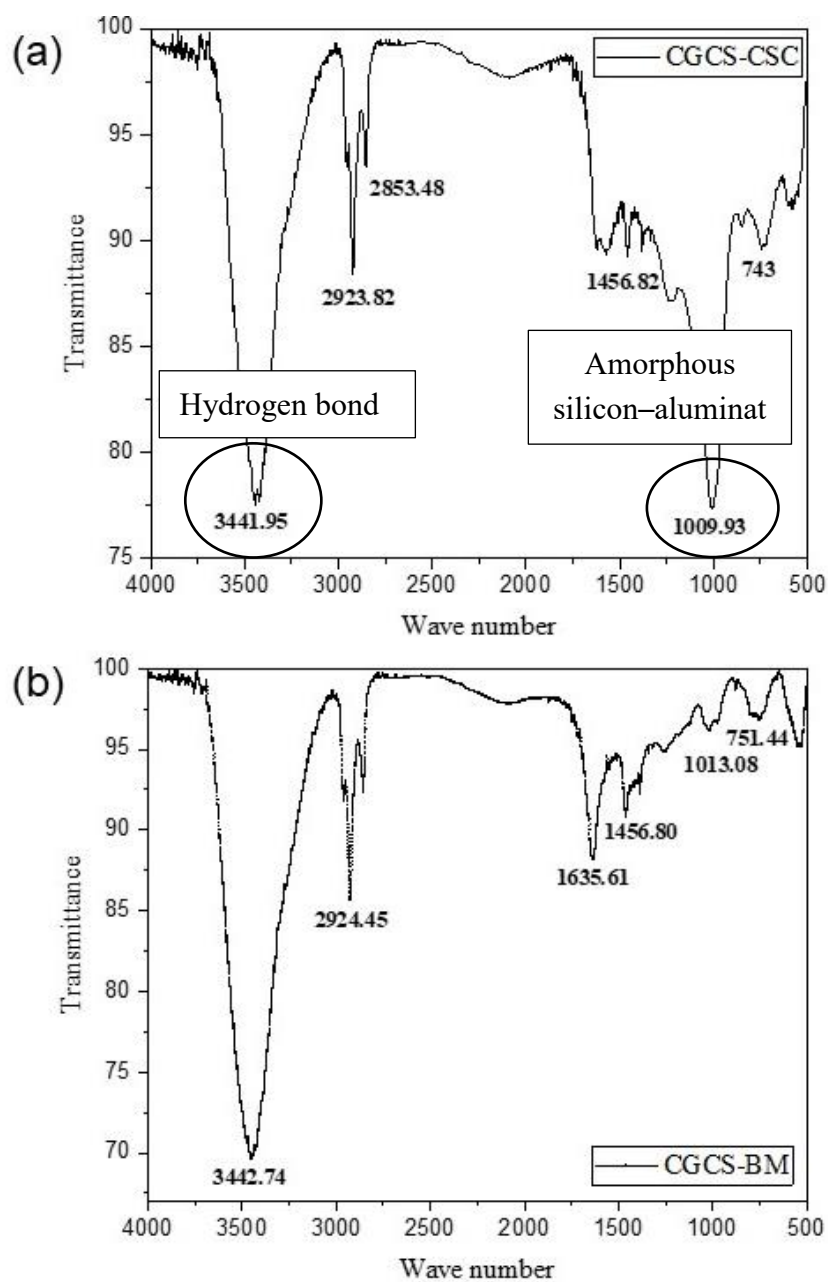
Figure 4. 5 FTIR about different peaks: (a) CGCS–CSC; (b) CGCS–BM.

There is a broad vibrational peak in it at around 3400 cm^{-1}, which may indicate the hydroxyl group in the water[59]. However, in the case of a completely dry sample and KBr, this vibrational peak shows peak changes in CGCS–CSC and CGCS–BM, indicating the presence of strong hydrogen bonds and partial physisorption of water

within the system. These silica hydroxyl groups are more likely to form siloxane bridges when the calcination temperature is gradually increased. The spectrum shows a small broad band near 1010 cm^{-1} corresponding to Si–O–Si or Al–O–Al, C–O stretching vibration of phenol, the C–N stretching vibration of amine, and the N–H deformation vibration of amine. C–N stretching vibration of amine, N–H deformation vibration, showing a typical amorphous silicon一aluminate structure [2]. There is a peak near 1400 cm^{-1}, which may represent the carbonyl group. Due to the large electric dipole moment of the carbonyl group, the absorption is generally strong.

In addition, the characteristic peak at 3740 cm^{-1} does not appear, indicating the absence of weak hydrogen bonds. Based on the analysis, it can be concluded that the type of silica hydroxyl groups on the CGCS–CSC surface is mainly adjacent to hydroxyl groups, probably due to the construction of more fine pores, but it cannot be excluded that some free hydroxyl groups may exist in the large pore size region.

5. ADSORPTION PERFORMANCE OF CGCS–CSC

5.1. Response Surface Methodology

The response surface methodology (RSM) is based on Central Composite Face centered in Design Expert 11. Five influencing factors were initially selected to investigate their effect on the removal capacity of CGCS–CSC: pH, MB concentration, reaction time, reaction temperature, and the amount of CGCS–CSC added. While 3^5 sets of data would have been required to produce results according to the orthogonal method, it only requires 46 sets of tests, which effectively reduces the number of experiments and allows the effect of multiple variables on the material to be efficiently accomplished through in-house calculations.

Table 5. 1 Fit summary of the fitting method in the first response surface methodology (five influencing factors) model

Fitting method	Sequential p–value	Lack of fit p–value	Adjusted R^2	Predicted R^2
Linear	< 0.0001	0.7914	0.7567	0.7165
2FI	0.0002	0.9824	0.8789	0.8715
Quadratic	**0.3127**	**0.9879**	**0.8848**	**0.8006**
Cubic	0.7354	0.9917	0.8603	0.4528

The pH 4–8, temperature 35–55 ºC, time 60–140 min, MB concentration 80–115 mg/L and CGCS–CSC addition 0.1–0.2 g. The change in adsorbance of MB was measured to obtain the change in adsorption volume, and the fit values of the five factors model

were obtained as shown in Table 5.1. The higher the adjusted R^2, the better the fit. Therefore, the Quadratic model was selected and fitted. The optimum conditions predicted by the model were pH 8, temperature 35 $^{\circ}$C, time 140 min, MB concentration 115 mg/L, and maximum adsorption of 726 mg/g for a CGCS–CSC addition of 1 g/L. Experimental validation was carried out under such conditions, yielding an MB removal capacity of 976 mg/g. This is very different from the predicted value. This may be because this method mainly uses experiments with variables $\leqslant$ 3. When there are more than three influencing factors, there may be a synergistic effect between the substances, leading to an error between the predicted and measured values.

In addition, when the MB concentration was 115 mg/L, the adsorbed solution changed from blue to almost colorless, indicating that the MB was completely adsorbed after the addition of 0.1 g CGCS–CSC. Therefore, the MB concentration should be increased appropriately to accurately determine the adsorption capacity of CGCS–CSC on MB. Moreover, according to the possible reaction mechanisms proposed in the literature, alkaline conditions favor the adsorption reaction, so the adsorption reaction should be evaluated at pH > 7.

Therefore, the influencing factors and ranges were reselected to perform a second experiment on the adsorption capacity of CGCS–CSC on MB. The influencing factors and ranges were: pH 7–11, MB concentration of 100–300 mg/L, CGCS–CSC addition of 0.05–0.15 g, reaction time fixed at 150 min, and reaction temperature at room temperature. The prediction equation for methylene blue elimination rate is Y after multiple regression equation fitting:

$$Y = 195.98 + 2.60A + 125.00B - 119.5C - 1.38AB + 0.375AC - 66.88BC \qquad (7)$$

Where A, B, and C denote the pH, MB concentration (mg/L), and quantity of CGCS–CSC added (g), respectively.

In the second RSM adsorption experiment, the real and anticipated adsorption results of MB are shown in Figure 5.1. Most of the experimental results are on a straight line, indicating that the regression model predicts the removal capacity of MB based on actual measurements. The R^2 of the MB removal capacity was 0.995 according to the model, indicating that this regression model can be used to estimate the theoretical adsorption of CGCS–CSC to MB.
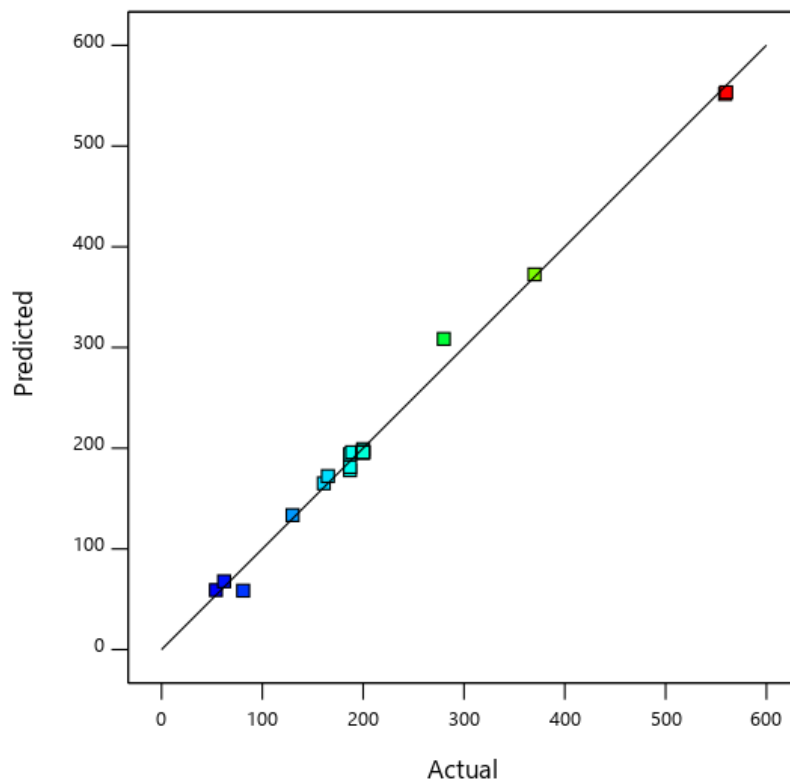

Figure 5. 1 Plot of predicted vs. actual for the adsorption process of MB

The removal capacity of CGCS–CSC for MB was optimized using Design Expert 11, and the best process conditions were determined as follows: the pH was 7, the starting

MB concentration was 300 mg/L, and the addition of CGCS–CSC was 0.05 g. The experimental removal capacity reached 556 mg/g, with a 0.29% deviation from the model's predicted value (554 mg/g). The predicted values of the model are closely associated with the measured values, allowing it to be correctly and reliably applied to the adsorption of cationic dyes by modified gasification slag. Simultaneously, under ideal circumstances, the removal capacity of CGCS–CSC for MB is approximately four times higher than that of other materials (shown in Table 5.2).

Table 5. 2 Comparison of S_{BET} and MB removal capacity of different materials

Material	S_{BET} (m^2/g)	Removal capacity (mg/g)	Refs.
CGCS–CSC	438	556	This study
FS–MGS	364	141	[10]
Carbon–CoFe$_2$O$_4$	463	120	[20]
Carbon/X zeolites	295	94	[23]

5.2. Effect of HCl Concentration on MB Removal Capacity

Acid leaching is an essential part of the preparation of carbon–silicon composites, the purpose of which is to leach out the metal oxides from them and form pore structures that act on the adsorption process. The BET surface area and the removal capacity of 300 mg/L MB solution were measured after acid leaching with 4, 8, 12, 16, and 20 wt% HCl at room temperature for 3 h, and the results are shown in Table 5.3. The maximum BET surface area and MB removal capacity were 438 m^2/g and 556 mg/g at 16 wt% HCl concentration, respectively. As shown in Figure 5.2, the amount of MB adsorption increased from 194 to 509 mg/g, and the BET surface area increased from 305 to 394

m^2/g with the increase in HCl concentration, but both BET surface area and MB removal capacity decreased when the HCl concentration exceeded 16 wt%.

Table 5. 3 The BET surface area and the removal capacity of 300 mg/L MB solution

HCl concentration (wt.%)	Removal Capacity (mg/g)	S_{BET} (m^2/g)
4	194	305
8	269	305
12	388	316
16	509	394
20	349	374
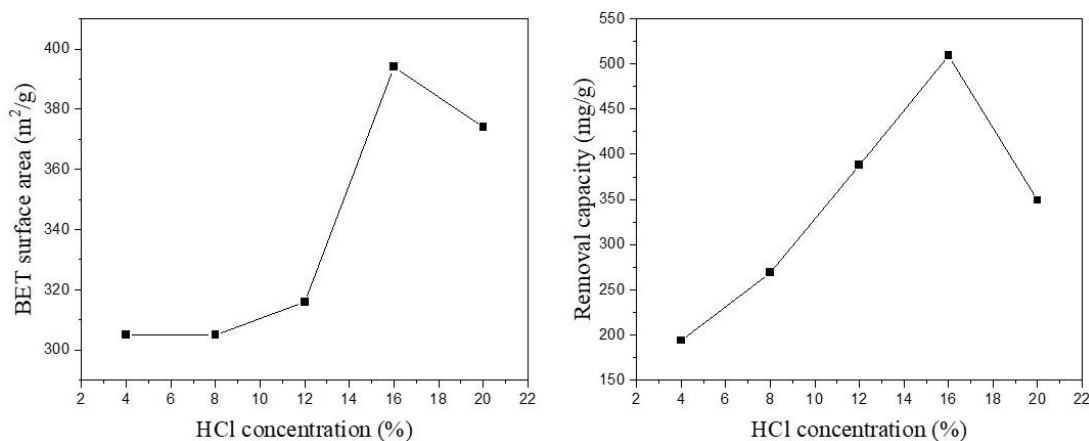
Figure 5. 2 Effect of HCl concentration on BET surface area and MB removal capacity.

The reason may be that HCl is a strong acid and has a faster rate or more violent reaction in leaching metal oxides, which can easily cause pore collapse, resulting in reduced BET surface area and decreased MB removal capacity. Therefore, 16 wt% HCl was selected for acid leaching in this thesis.

5.3. Effect of pH on MB Removal Capacity

The joint effect of different pH and other factors on MB adsorption was tried in response surface methodology, but the results showed that there was no interaction between these factors, so the effect of pH on the capacity of MB adsorption was explored.

The variable pH range of 2–11 was chosen for the experiment, other conditions were MB concentration of 300 mg/L, the addition of 0.5 g/L CGCS–CSC, and adsorption time of 150 min. Figure 5.3 shows MB adsorption increased with increasing pH, indicating that the alkaline conditions were favorable for the adsorption to proceed. However, at $pH \geq 7$, MB adsorption increased slowly. Therefore, to reduce water pollution and affect the normal life of other aquatic organisms, $pH = 7$ was selected for the conditions.
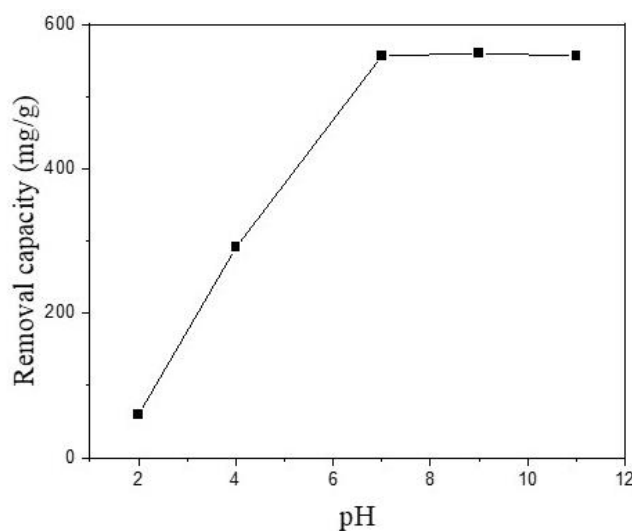
Figure 5. 3 Effect of pH on MB removal capacity

5.4. Effect of MB Concentration on MB Removal Capacity

Different MB concentrations also affect the effectiveness of the MB removal rate within

the system. In this work, we tried the adsorption of 100–600 mg/L MB solution. Other

conditions were: pH = 7, addition of 0.5 g/L CGCS–CSC, and adsorption time 150 min.

As shown in Figure 5.4, the slope of MB removal capacity increased and then decreased

with the increase of MB concentration. This indicates that saturation of adsorption can

be achieved by adding 0.5 g/L of CGCS–CSC when the MB concentration is 300 mg/L.
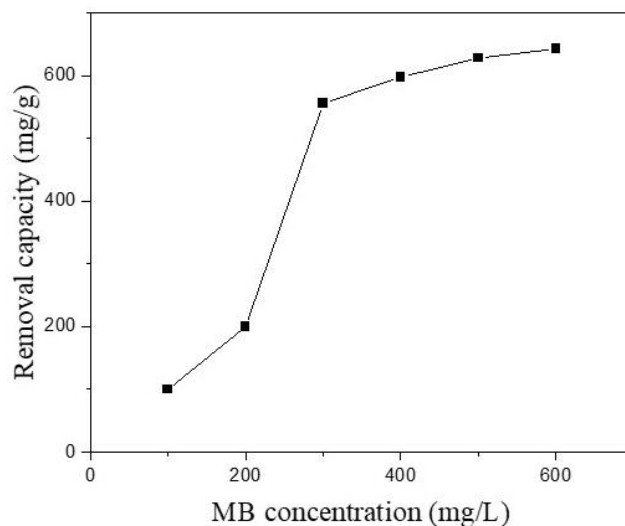
Figure 5. 4 Effect of MB concentration on MB removal capacity

6. MECHANISM OF MB ADSORPTION

6.1. Surface Chemical Activated Groups

Another factor that affects the MB removal capacity of a material is the amount of surface–active groups. Sun [60] stated that the condensation of silicone hydroxyl groups removes one molecule of water. Figure 1.3 depicts in detail the structures and properties of the different surface–active groups, and only two structures (a) isolated silanol groups and (b) genimal silanol groups (shown in Figure 1.3) are consistent with this assertion. Therefore, in this study, TGA was used to calculate the amount of surface–active groups via the measurement of weight loss of the water in the sample. In this work, TGA was performed under the condition that 20 mg of the dried sample was placed in a crucible, rising at a rate of 10 °C/min in the temperature range of 180–1100 °C under N_2 atmosphere. The weight change of CGCS–CSC was calculated.

Table 6. 1 Comparison of N_{OH} and S_{BET} of different samples

Sample	N_{OH} (/nm^2)	S_{BET} (m^2/g)	Ref.
CGCS–CSC	$24.0 < N_{OH} < 26.5$	438	This study
MGS1	1.2	364	[60]
MS–1	9.1	727	[60]
MS–2	7.3	660	[60]
MS–3	6.9	631	[60]
MS–4	6.4	585	[60]

Table 6.1 compares the N_{OH} and S_{BET} of different materials and it can be seen that the N_{OH} and S_{BET} of CGCS–CSC are proportional. The equation for the calculation of N_{OH}

[56] shows the following:

$$N_{OH} = \frac{W_{OH} \times 2 \times 10^3}{3 \times S_{BET}}$$

(8)

Where W_{OH} is weight loss (%), S_{BET} is BET surface area (m^2/g).
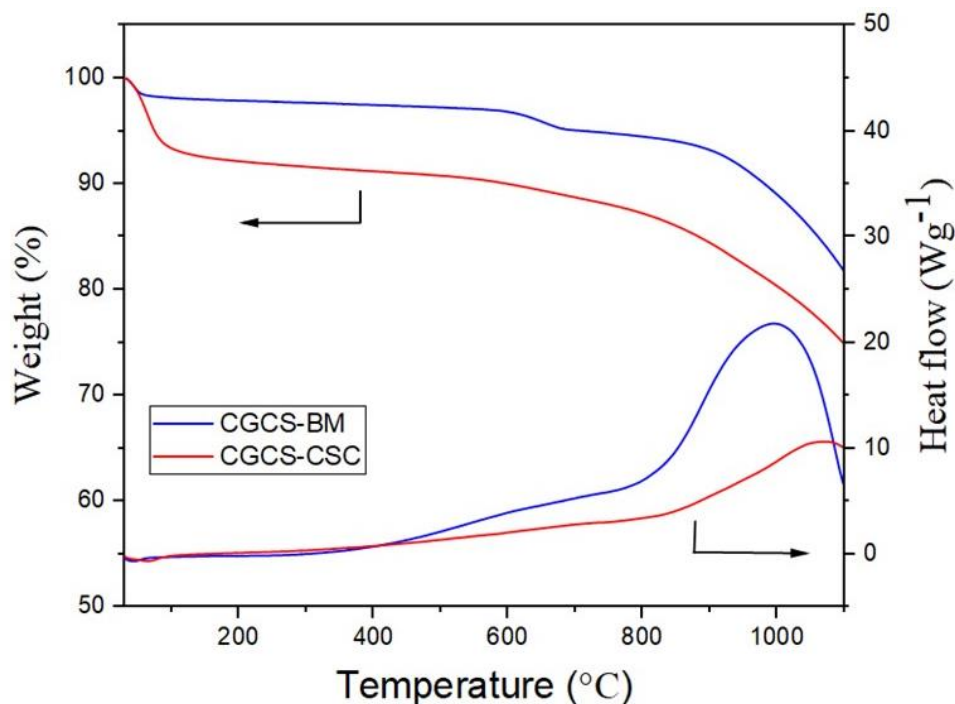
Figure 6. 1 TGA of samples under N$_2$ atmosphere

Figure 6.1 shows the weight loss of CGCS–CSC under N$_2$. Under the N$_2$ atmosphere, the water involved in the CGCS–BM has completely evaporated when the temperature exceeds 180 ºC, at which point only one form of water is present in the reaction process, that is, the water molecules formed when the surface reactive groups are bound to MB$^+$ [11]. However, during this process, the residual carbon reacts with the activated Fe metal at about 300–600 ºC [42], producing a partial weight loss. The weight loss at 180–1100 ºC was 17.4% (from 92.3% to 74.9%) and at 300–600 ºC was 1.6% (from 91.6% to 90.0%). Calculated by the equation (8), the amount of silica hydroxyl groups is between 24.0 and 26.5 /nm^2.

The amount of silica hydroxyl groups is the same as the calculation method proposed by Liu [9]. After comparison, the amount of silica hydroxyl groups in CGCS–CSC is much larger than that of other materials. This may be the main reason why the removal capacity of MB by CGCS–CSC can reach 556 mg/g.

6.2. Kinetics and Thermodynamics

6.2.1. Adsorption Isotherms

The adsorption isotherm is the relationship between the amount of MB solution adsorbed by CGCS–CSC and the equilibrium concentration of solution after adsorption by measuring a certain temperature and pH. Langmuir and Freundlich were used to simulating the adsorption process of methylene blue on CGCS–CSC. The equations of the two models are shown below:

Freundlich Model:

$$Q_e = k_f C_e^{\frac{1}{n}} \tag{9}$$

Where k_f and n are related to removal capacity (mg/g) and adsorption intensity of the system; C_e is MB concentration (mg/L).

Langmuir Model:

$$Q_e = \frac{Q_L k_L C_e}{1 + k_L C_e} \tag{10}$$

Where Q_L is the maximum removal capacity (mg/g); k_L is the Langmuir constant; C_e is MB concentration (mg/L).
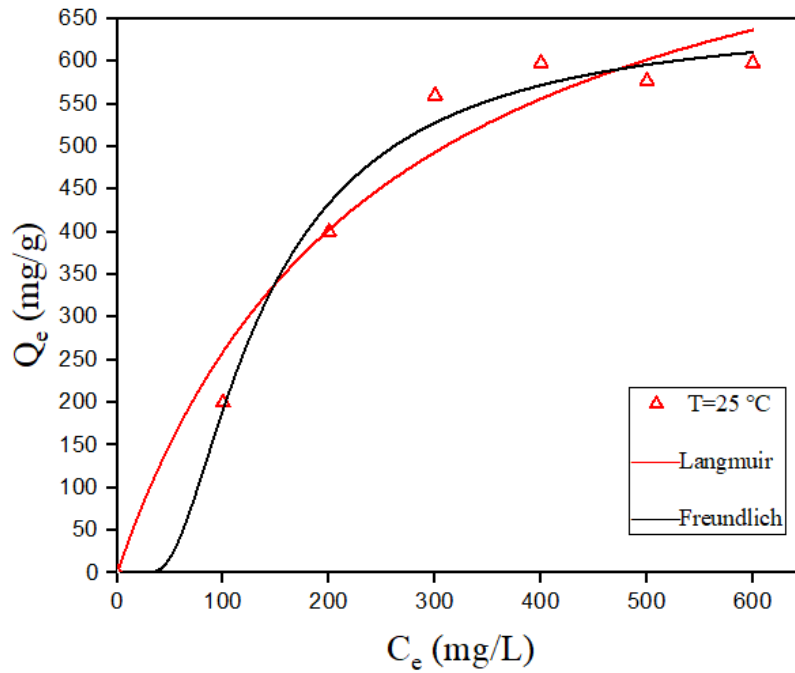
Figure 6. 2 Equilibrium adsorption isotherm of methylene blue onto CGCS–CSC at different temperatures

The fitting of the two models are illustrated in Figure 6.2, and the parameters are shown in Table 6.2. The results reveal that the experimental data fit the Langmuir model better than the Freundlich model, with a good fitting determination coefficient (R^2=0.994). The Langmuir model suggests that the process is a single molecular layer adsorption process. This means that the monolayer of CGCS–CSC covers a homogeneous surface during the adsorption process and there are no subsequent interactions.

Table 6. 2 Thermodynamic model fitting parameters for the MB adsorption onto CGCS–CSC

	Langmuir			Freundlich		
	R^2	Q_L (mg/g)	k_L (L/mg)	R^2	k_f (mg/g)	n
25 ℃	0.994	556	37.0	0.955	553	9.07

6.2.2. Adsorption Kinetics

Pseudo–first–order kinetic model refers to a model method in which the reaction rate has a linear relationship with the concentration of a reactant. Physical adsorption is the main adsorption process, that is, the interaction between adsorbent and solute exists on the surface. The equation is as follows:

$$q_t = q_e - q_e e^{-k_1 t} \tag{11}$$

Where q_e and q_t (mg/g) are the amount of methylene blue solution adsorbed by the adsorbent at equilibrium state and time t (min) respectively, and k_1 is a constant.

To verify whether it is chemisorption, the pseudo–second–order kinetic model verifies whether the occupation rate of the adsorption site is proportional to the square of unoccupied sites, and its equation is as follows:

$$q_t = \frac{k_2 q_e^2 t}{1 + K q_e t} \tag{12}$$

Where q_e and q_t (mg/g) are the amount of methylene blue solution adsorbed by the adsorbent at equilibrium state and time t (min) respectively, and k_2 is a constant.
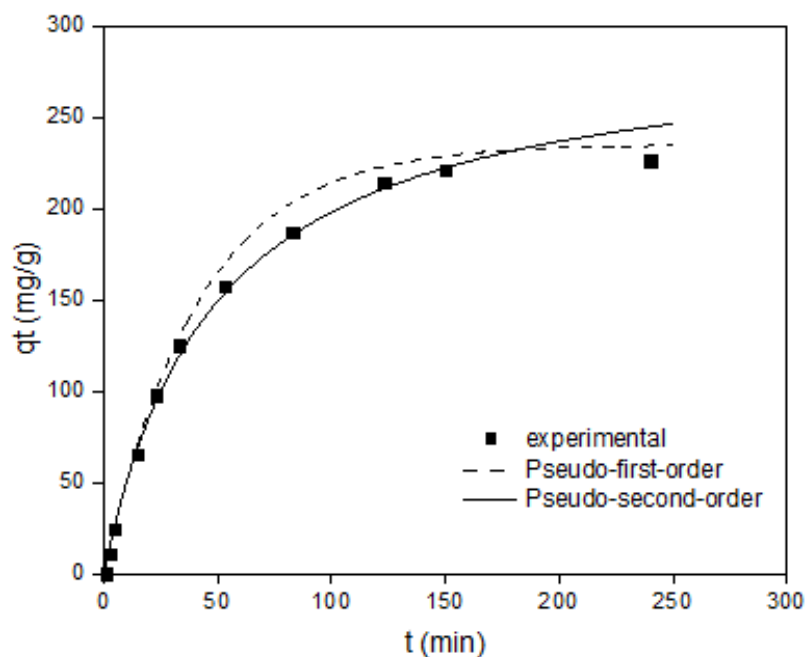
Figure 6. 3 Equilibrium adsorption isotherm of methylene blue onto CGCS–CSC at room temperature

Figure 6.3 shows the fitting of experimental data to two kinetic models, and the corresponding parameters are given in Table 6.3. On the other hand, the fitted results are consistent with the Pseudo–first–order kinetics, indicating that the MB adsorption on CGCS–CSC is physisorption, which may be due to hydrogen bonding and electrostatic interaction and MB^+ [11].

Table 6. 3 Kinetic model fitting parameters for the MB adsorption onto CGCS–CSC

First–order	q_e (mg/g)	k_1 (min^{-1})	R^2
	235	0.02	0.998
Second–order	q_e (mg/g)	k_2 (g mg^{-1} min^{-1})	R^2
	294	0.00003	0.991

7. CONCLUSIONS AND PROSPECTS

In conclusion, the morphological characteristics, substance changes, as well as different factors affecting the removal capacity of methylene blue, were investigated by SEM–EDS, XRD, and response surface method (RSM), respectively. SEM–EDS analysis showed that CGCS–CSC is mostly composed of mesoporous silica and mesoporous carbon s with well-developed pores. Elements such as Si, Al, Fe, Ca, Na, and S are present in the tiny regions of the particles, while most of the regions are covered by carbon. XRD results show that the modified CGCS–CSC appears to have a distinct phase of SiO_2, which indicates that a typical structure of mesoporous silica is formed in the system. The effect of different factors on the removal capacity of methylene blue was investigated by RSM. Among them, HCl concentration, pH, and MB concentration play an important role on the MB removal capacity.

In addition, the characteristic FTIR peaks around 3450 and 1010 cm^{-1} indicate that the synthesized material features a structure of physisorbed water, strong hydrogen bonding, and mesoporous silica. Based on the measured BET surface area (438 m^2/g) and the amount of surface–active groups (between 24.0 and 26.5 /nm^2), it can be inferred that the adsorption of methylene blue by CGCS–CSC mainly proceeds through hydrogen bonding and electrostatic interaction. The maximum removal capacity of methylene blue tested under optimal conditions was 556 mg/g.

As the research on carbon in coal gasification slag is insufficient, such as the morphological changes and surface chemical properties of carbon. Hence, it is necessary to study its mechanisms via a series of testing to lay a good foundation for

the rational utilization of the carbonaceous components in it; Meanwhile, gasification slag is receiving a lot of attention in the manufacture of ceramic materials and aluminum/silicon–based products, among other things. It is, however, still at the laboratory stage and cannot be put into mass production. Thus, developing a robust and low cost modification method is an efficient solution to fulfill the present urgent need for gasification slag utilization.

REFERENCES

[1] Guo, Q. Guangsuo, Y. Wang, F. Wang, Y., & Dai, Z. Opposed Multi-Burner (OMB) Coal-Water Slurry Gasification Technology and its Industrial Applications, Energy Procedia, 142 (2018) 1089-1094.

[2] W. Yang. Z. Sshiyong. L. Bo, Study on the residue features of Ningdong coal in entrained flow gasifiers, Coal Engineering, 49 (2017).

[3] L.C.A. Oliveira, M. Gonçalves, M.C. Guerreiro, T.C. Ramalho, J.D. Fabris, M.C. Pereira, K. Sapag, A new catalyst material based on niobia/iron oxide composite on the oxidation of organic contaminants in water via heterogeneous Fenton mechanisms, Applied Catalysis A: General, 316 (2007) 117-124.

[4] C. Pan, Q. Liang, X. Guo, Z. Dai, H. Liu, X. Gong, Characteristics of Different Sized Slag Particles from Entrained-Flow Coal Gasification, Energy & Fuels, 30 (2016) 1487-1495.

[5] C.S. Castro, M.C. Guerreiro, M. Goncalves, L.C. Oliveira, A.S. Anastacio, Activated carbon/iron oxide composites for the removal of atrazine from aqueous medium, Journal of Hazard Mater, 164 (2009) 609-614.

[6] C. Jiquan, Development of textile auxiliaries industry at home and abroad, Fine and Specialty Chemicals, (2010).

[7] K. Zhang, L. Van Dyk, D. He, J. Deng, S. Liu, H. Zhao, Synthesis of zeolite from fly ash and its adsorption of phosphorus in wastewater, Green Processing and Synthesis, 10 (2021) 349-360.

[8] G. Fadillah, T.A. Saleh, S. Wahyuningsih, E. Ninda Karlina Putri, S. Febrianastuti, Electrochemical removal of methylene blue using alginate-modified graphene adsorbents, Chemical Engineering Journal, 378 (2019).

[9] S. Liu, X. Chen, W. Ai, C. Wei, A new method to prepare mesoporous silica from coal gasification fine slag and its application in methylene blue adsorption, Journal of Cleaner Production, 212 (2019) 1062-1071.

[10] L.T. Zhuravlev, The surface chemistry of amorphous silica. Zhuravlev model., Colloids and Surfaces, A: Physicochemical and Engineering Aspects 173 (2000) 2001-2038.

[11] Y. Yao, F. Xu, M. Chen, Z. Xu, Z. Zhu, Adsorption behavior of methylene blue on carbon nanotubes, Bioresoure Technology, 101 (2010) 3040-3046.

[12] M.A. Al-Ghouti, M.A. Khraisheh, S.J. Allen, M.N. Ahmad, The removal of dyes from textile wastewater: a study of the physical characteristics and adsorption mechanisms of diatomaceous earth, Journal of Environmental Management, 69 (2003) 229-238.

[13] X. Shang, M. Jianli, J. Zhang, X.U. Danyu, L. Zhang, J. Zhou, Research status and prospects of utilization technologies of slag from coal gasification, Journal of Environmental Engineering Technology., 7 (2017) 712-717.

[14] T. Wu, M. Gong, E. Lester, F. Wang, Z. Zhou, Z. Yu, Characterisation of residual carbon from entrained-bed coal water slurry gasifiers, Fuel, 86 (2007) 972-982.

[15] Y. Tang, H. Yin, H. Yuan, H. Shuai, Y. Xin, Phase and morphological transformation stages during carbothermal reduction nitridation process: From coal gasification slag wastes to Ca-α-SiAlON powders, Advanced Powder Technology, 27 (2016) 2232-2237.

[16] W. Ji, S. Zhang, P. Zhao, S. Zhang, N. Feng, L. Lan, X. Zhang, Y. Sun, Y. Li, Y. Ma, Green Synthesis Method and Application of NaP Zeolite Prepared by Coal Gasification Coarse Slag from Ningdong, China, Applied Sciences, 10 (2020).

[17] N. Yuan, A. Zhao, Z. Hu, K. Tan, J. Zhang, Preparation and application of porous materials from coal gasification slag for wastewater treatment: A review, Chemosphere, 287 (2022).

[18] K. Wu, C. Ji, L. Luo, X. Wang, Simulation Study of Moon-Based InSAR Observation for Solid Earth Tides, Remote Sensing, 12 (2020).

[19] D. Li, H. Min, X. Jiang, X. Ran, L. Zou, J. Fan, One-pot synthesis of Aluminum-containing ordered mesoporous silica MCM-41 using coal fly ash for phosphate adsorption, Journal of Colloid and Interface Science, 404 (2013) 42-48.

[20] Z.Y. Yao Zhipeng, W. Hui, W. Maoling, H. Yuming, Removal of Rhodamine B by an Activated Carbon-$CoFe_2O_4$ Magnetic Nanocomposite, Journal of Southwest University (Natural Science Edition), (2015).

[21] Q.J. ZHANG G. aosheng, L. Huijuan, L. Ruiping, W. Rongcheng, Magnetic adsorbents: activated carbon /iron oxide composites for AO7 removal from aqueous system, Acta Scientiae Circumstantiae, (2006) 26(11):1763-1768.

[22] K. Xia, Y. Guo, Q. Shao, Q. Zan, R. Bai, Removal of Mercury (II) by EDTA-Functionalized Magnetic $CoFe_2O_4@SiO_2$ Nanomaterial with Core-Shell Structure, Nanomaterials (Basel), 9 (2019).

[23] L.B. Amine Khelifa, Zoubir Derriche, Adsorption of carbon dioxide by X zeolites exchanged with Ni^{2+} and Cr^{3+}: isotherms and isosteric heat, Colloid and Interface Science, Oct 1 (2004) 278(271):279-217.

[24] Z. Tingting, Y. Yanling, L. Xing, J. Yifan, W. Nan, J. Siyang, Z. Zhiwei, Adsorption characteristics and mechanism of azo dyes by powdered activated carbon, Journal of Central South University, 50 (2019).

[25] A. Azimi, A. Azari, M. Rezakazemi, M. Ansarpour, Removal of Heavy Metals from Industrial Wastewaters: A Review, ChemBioEng Reviews, 4 (2017) 37-59.

[26] S. Xu, Y. Lv, X. Zeng, D. Cao, ZIF-derived nitrogen-doped porous carbons as highly efficient adsorbents for removal of organic compounds from wastewater, Chemical Engineering Journal, 323 (2017) 502-511.

[27] M. Wdowin, M. Franus, R. Panek, L. Badura, W. Franus, The conversion technology of fly ash into zeolites, Clean Technologies and Environmental Policy, 16 (2014) 1217-1223.

[28] T. Zhu, X. Zhang, Y. Han, T. Liu, B. Wang, Z. Zhang, Preparation of Zeolite X by the Aluminum Residue From Coal Fly Ash for the Adsorption of Volatile Organic Compounds, Frontiers in Chemistry, 7 (2019) 341.

[29] M. Smolilo, K. Samson, T. Zhou, D. Duraczynska, M. Ruggiero-Mikolajczyk, A. Drzewiecka-Matuszek, D. Rutkowska-Zbik, Oxidative Dehydrogenation of Propane over Vanadium-Containing Faujasite Zeolite, Molecules, 25 (2020).

[30] Y.K. Krisnandi, F.M. Yanti, S.D.S. Murti, Synthesis of ZSM-5 zeolite from coal fly ash and rice husk: characterization and application for partial oxidation of methane to methanol, Materials Science and Engineering, 188 (2017).

[31] Y. Zhang, J. Dong, F. Guo, Z. Shao, J. Wu, Zeolite Synthesized from Coal Fly Ash Produced by a Gasification Process for Ni^{2+} Removal from Water, Minerals, 8 (2018).

[32] A. Molina, C. Poole, A comparative study using two methods to produce zeolites from fly ash, Minerals Engineering, 17 (2004) 167-173.

[33] A. Firouzi, D. Kumar, L.M. Bull, T. Besier, P. Sieger, Q. Huo, S.A. Walker, J.A. Zasadzinski, C. Glinka, J. Nicol, Cooperative organization of inorganic-surfactant and biomimetic assemblies, Science, 267 (1995) 1138.

[34] J. Stjernberg, M.A. Olivas-Ogaz, M.L. Antti, J.C. Ion, B. Lindblom, Laboratory scale study of the degradation of mullite/corundum refractories by reaction with alkali-doped deposit materials, Ceramics International, 39 (2013) 791-800.

[35] C.c. Li, X.c. Qiao, J.g. Yu, Large surface area MCM-41 prepared from acid leaching residue of coal gasification slag, Materials Letters, 167 (2016) 246-249.

[36] H. Wenhao, Z. Jianbo, L. Shaopeng, L. Zhanbing, S. Zhigang, Huiquan, S. Zhigang, Study on the preparation of polyaluminium chloride from coal gasification residue, Clean Coal Technology, 25 (2019).

[37] A. Okoye, P. Ejikeme, O. Onukwuli, Lead removal from wastewater using fluted pumpkin seed shell activated carbon: Adsorption modeling and kinetics, International Journal of Environmental Science & Technology, 7 (2010) 793-800.

[38] Z. Zhang, Y. Zhang, J. Zhang, Y. Li, Y. Ma, C. Xu, Effect of ZRB2-modified on microstructure and mechanical properties of Mg-Zn-Y-Mn alloy, Journal of Magnesium and Alloys, 6 (2018) 255-262.

[39] Y. Xu, X. Chai, Characterization of coal gasification slag-based activated carbon and its potential application in lead removal, Environmental Technology, 39 (2018) 382-391.

[40] Z. Lei, Y. Xiao, L. Dang, S. Bai, L. An, Graphitized carbon with hierarchical mesoporous structure templated from colloidal silica particles, Microporous and Mesoporous Materials, 109 (2008) 109-117.

[41] T. Horikawa, S. Tan, D.D. Do, K.-I. Sotowa, J.R. Alcántara-Avila, D. Nicholson, Temperature dependence of water adsorption on highly graphitized carbon black and highly ordered mesoporous carbon, Carbon, 124 (2017) 271-280.

[42] J. Sreńscek-Nazzal, W. Kamińska, B. Michalkiewicz, Z.C. Koren, Production, characterization and methane storage potential of KOH-activated carbon from sugarcane molasses, Industrial Crops and Products, 47 (2013) 153-159.

[43] Y.y. Gu, X.c. Qiao, A carbon silica composite prepared from water slurry coal gasification slag, Microporous and Mesoporous Materials, 276 (2019) 303-307.

[44] D. Zhu, J. Zuo, Y. Jiang, J. Zhang, J. Zhang, C. Wei, Carbon-silica mesoporous composite in situ prepared from coal gasification fine slag by acid leaching method and its application in nitrate removing, Science of The Total Environment, 707 (2020) 136102.

[45] D. Nandan, P. Sreenivasulu, L.N. Sivakumar Konathala, M. Kumar, N. Viswanadham, Acid functionalized carbon–silica composite and its application for solketal production, Microporous and Mesoporous Materials, 179 (2013) 182-190.

[46] Y. Fang, G. Zheng, J. Yang, H. Tang, Y. Zhang, B. Kong, Y. Lv, C. Xu, A.M. Asiri, J. Zi, F. Zhang, D. Zhao, Dual-pore mesoporous carbon@silica composite core-shell nanospheres for multidrug delivery, Angewandte Chemie International Edition, 53 (2014) 5366-5370.

[47] H. Tian, M. Saunders, A. Dodd, K. O'Donnell, M. Jaroniec, S. Liu, J. Liu, Triconstituent co-assembly synthesis of N,S-doped carbon–silica nanospheres with smooth and rough surfaces, Journal of Materials Chemistry A, 4 (2016) 3721-3727.

[48] D. Barpaga, M.D. LeVan, Functionalization of carbon silica composites via in‑pore synthesis of active sites for NH_3 and SO_2 adsorption, Adsorption, 23 (2017) 779-787.

[49] H. Yang, W. Yang, K. Lv, J. Zhu, Y. Xia, D. Tang, L. Wen, Effect of the structure of CN/Silica composite support on the catalytic performances of Co_3O_4 for CO oxidation, Microporous and Mesoporous Materials, 255 (2018) 36-43.

[50] H. Heidari, C. Mammostafaei, Spectrophotometric determination of lamotrigine in plasma samples: Ultrasound-assisted emulsification-microextraction based on a hydrophobic deep eutectic solvent followed by back-extraction, Spectrochimica Acta, Part A: Molecular and Biomolecular Spectroscopy, 247 (2021) 119098.

[51] A. Salehi, E. Najafi Kani, Green cylindrical mesoporous adsorbent based on alkali-activated phosphorous slag: synthesis, dye removal, and RSM modeling, Adsorption, 24 (2018) 647-666.

[52] Y. Zhao, X. Jin, X. Zhou, A Novel Photodiode for Ultraviolet Spectral Range 2012 International Conference on Electronic Information and Electrical Engineering, Atlantis Press, Changsha, Hunan, China, 2012.

[53] L. Qiang, Z. Xuehua, C. Sihai, Z. Jianhou, Y. Tianbang, Determination of twenty components in cobalt-rich crust samples by X-ray fluorescence spectrometry with high-pressure powder pelleting preparation, Metallurgical Analysis, 41 (2021) 20-26.

[54] G. Lixi, BET Analysis of Physical Properties of Porous Material, www.gdchem.com, 48 (2021).

[55] W. Peng, The Attempts in Adding Contents of Science and Application of Adsorption into Teaching Courses of Physical Chemistry for Engineering Majors, www.gdchem.com, 47 (2020).

[56] L. Yanduan, Study on the removal of Hg^0 from flue gas by coal dry powder gasification coarse slag, Petrochemical Industry Technology, (2019).

[57] X. Zhang, Y. Wu, X. Li, X. Meng, H. Shi, Z. Wu, J. Zhang, Preparation of mesoporous silica from coal slag and its metal ion adsorption behavior, Korean Journal of Chemical Engineering, 36 (2019) 753-762.

[58] Y. Xianglian, Y. Qiang, M. Yulong, H. Shukai, Q. Rubin, L. Xintian, Z. Xiaozhe, W. Qianqian, Detection of SF_6 Decomposition Product SO_2F_2 in GIS Gas Chamber Based on FTIR, Advanced Sensor Systems and Applications XI, 43 (2021) 1393-1398.

[59] P. Yuan, D.Q. Wu, H.P. He, Z.Y. Lin, The hydroxyl species and acid sites on diatomite surface: a combined IR and Raman study, Applied Surface Science, 227 (2004) 30-39.

[60] S. Zhenhai, L. Bin, G. Chunlei, Z. Jiazhong, L. Ben, F. Jingxin, W. Yang, Study on synthesis of mesoporous silica and its adsorption and separation properties, Inorganic Chemicals Industry, 53 (2021).